Pathological Study on the Possible Translocation Pathways of the Exposed Nanoparticles at the Air–Blood Barrier under the Inflammatory Condition Induced by Asian Sand Dust and at the Maternal–Fetal Barrier during Pregnancy in Mice

黄砂に曝露され炎症状態にある肺の血液空気関門および妊娠マウスの血液胎盤関門におけるナノ粒子の関門突破機序についての病理学的研究

Kasem Rattanapinyopituk

Thesis submitted to the United Graduate School of Veterinary Science at Yamaguchi University in partial fulfillment of the requirements for the degree of Doctor of Philosophy

Takehito Morita, Ph.D., Chair
Akihiko Sugiyama, Ph.D.
Toshiharu Hayashi, Ph.D.
Yoshiaki Yamano, Ph.D.
Tomohiro Imagawa, Ph.D.

The United Graduate School of Veterinary Science
Yamaguchi University

2014

ABSTRACT

Pathological Study on the Possible Translocation Pathways of the Exposed Nanoparticles at the Air–Blood Barrier under the Inflammatory Condition Induced by Asian Sand Dust and at the Maternal–Fetal Barrier during Pregnancy in Mice

Kasem Rattanapinyopituk

Nanotechnology is developing rapidly and is involved in a wide range of application. Therefore, the exposure to nanoparticles and their potential toxicity are of great concern. The potential hazard of nanoparticles is better to examine whether nanoparticles may access to the systemic circulation and reach the systemic organs, especially in the specific health conditions, e.g. during pulmonary injury induced by ambient air pollutions or during pregnancy. In the first chapter of the thesis, the possible translocation mechanisms of the intratracheally instilled gold nanoparticles at the air–blood barrier after the induction of acute pulmonary injury by Asian sand dust were investigated using Asian sand dust and gold nanoparticles. Lungs from mice treated with Asian sand particles and gold nanoparticles showed an acute focal inflammation with an increased expression of proinflammatory cytokines (IL-6 and TNF-α) and oxidative stress markers (Cu/Zn SOD and iNOS) in alveolar macrophages, type I alveolar epithelial cells and endothelial cells at the alveolar walls. Electron microscopy revealed a destruction of the alveolar walls with an increased number of endocytic vesicles in the cytoplasm of both type I epithelial cells and endothelial cells; gold nanoparticles were demonstrated in these endocytic vesicles. These findings suggest that translocation of the exposed nanoparticles may be enhanced in the lung tissues with acute inflammatory changes.

Fetuses are known to be susceptible to various exogenous substances, including nanoparticles. As the risk of exposure to nanoparticles in pregnancy increases, there are growing concerns about the effects of nanoparticles on pregnant woman and the possibility that nanoparticles can translocate through the placenta and cause toxicity to the fetus. In the second chapter, the possible translocation pathway of gold nanoparticles across the maternal–fetal barrier as well as the toxicity of intravenously administered gold nanoparticles to the placenta and fetus was examined. Pregnant ICR mice were intravenously administered with 20- and 50-nm gold nanoparticles on the 16^{th} and 17^{th} days of gestation. There was no sign of toxic damage to the placentas as well as maternal and fetal organs of the mice treated with 20- and 50-nm gold nanoparticles. ICP-MS analysis demonstrated significant amounts of gold deposited in the maternal livers and placentas but no detectable level of gold in the fetal organs. However, electron microscopy demonstrated an increase of endocytic vesicles in the cytoplasm of syncytiotrophoblasts and fetal endothelial cells in the maternal–fetal barrier of mice treated with gold nanoparticles. Clathrin immunohistochemistry and immunoblotting showed increased immunoreactivity of clathrin protein in the placental tissues of mice treated with 20- and 50-nm gold nanoparticles, and its immunopositivity was observed in syncytiotrophoblasts and fetal endothelial cells. In contrast, caveolin-1 immunopositivity was observed exclusively in the fetal endothelium. These findings suggest that intravenous administration of gold nanoparticles may upregulate clathrin- and cavelin-mediated endocytosis at the maternal–fetal barrier in mouse placenta.

This thesis obtained following two conclusions.

1. The translocation of the exposed nanoparticles may occur by injury of lung tissues due to acute inflammatory changes.
2. The intravenous administered gold nanoparticles may upregulate clathrin- and cavelin-mediated endocytosis at the maternal–fetal barrier. Clathrin- and caveolin-1

mediated endocytosis may be one of translocation pathway of nanopartilces at the maternal–fetal barrier in mouse placenta.

The information from the studies may be useful in assessing the risk of nanoparticle exposures, especially in the specific health conditions.

TABLE OF CONTENTS

GENERAL INTRODUCTION AND BACKGROUND

1. Nanoparticles

Nanoparticles had already been introduced into a daily life of people after the rapid development of nanotechnology. Nanoparticles had been used in various purposes such as biomedical applications, commercial products (e.g. foods, cosmetics, electronic devices), and industrial processes (De Jong et al. 2008; Lasagna-Reeves et al. 2010; Sadauskas et al. 2009a). While nanotechnology has made a remarkable development, the unexpected effects of nanoparticles are also growing concerned on the environment, health and society. Therefore, the impacts from intentional and accidental exposure are recognized as critical issues, which should be investigated and addressed to the public health (Figure 1) (Myojo et al. 2010; Ramachandran, 2011; Warheit et al. 2008; WHO 2003). Although several evidences from recent studies suggested that nanoparticles may have the effects on health, however, the information about cause-effect relationships remains unclear (Elsaesser and Howard 2012; Saunders 2009; Semmler-Behnke et al. 2008; Vega-Villa et al. 2008).

2. Characteristics of nanoparticles

Nanoparticles or ultrafine particles or $PM_{0.1}$ are defined as single particles with at least one dimension measuring 100 nm or less (De Jong et al. 2008; Yang et al. 2008). The dominant characteristic of nanoparticles is very small size that is different from those of fine ($PM_{2.5}$, particles larger than 0.1 μm and smaller than 2.5 μm) or coarse particles (PM_{10}, particles larger than 2.5 μm and smaller than 10 μm) (Ramachandran 2011; WHO, 2005; Yang et al. 2008). The smaller sized nanoparticles can exhibit unique physical and chemical properties of the particles such as large surface area per unit mass and unstable chemical bonds on surface of the particles. These properties of nanoparticles increase the reactivity on

the biological molecules that may cause greater toxicity after exposure (Ramachandran 2011; Saunders 2009). Therefore, the particles size and surface area of nanoparticles are crucial characteristics from toxicological aspect. Moreover, the particle surface chemistry, biodegradability, number, shape, and solubility are also significant factors in assessment of harmful biological effects (Yang et al. 2008). In addition, nanoparticles released into the environment interact with natural organic and inorganic substances often modified the surface properties of the nanoparticles, which can result the changes in nanoparticle properties (Elsaesser and Howard 2012).

3. Routes of exposure to nanoparticles

In general, it has been demonstrated that respiratory tract, skin and gastrointestinal tract are the significant routes of exposure of nanoparticles (Figure 2) (Elsaesser and Howard 2012; Vega-Villa et al. 2008).

3.1 Respiratory route

The lungs considered the most likely entry route through inhalation. Inhalation is important exposure route for the ambient air-borne nanoparticles. Nanoparticles can be deposited in all parts of the respiratory tract including the airways and the alveoli, however, smaller particles reach the distal part, whereas the larger particles may be eliminated by phagocytotic process in the upper respiratory tract (Furuyama et al. 2009; Saunders 2009).

3.2 Dermal route

Dermal exposure is also hypothesized to be the most common exposure route that can occur during the intentional purposes from the application of cosmetics, topical creams, and other drug treatments (Vega-Villa et al. 2008). The penetration of nanoparticles is depended on the characteristics of each nanoparticles, including surface coatings and geometric shapes of the particles (Ramachandran 2011).

3.3 Gastrointestinal route

Gastrointestinal tract exposure to nanoparticles occurred via the direct ingestion of nanoparticles (e.g. food additives, drugs, water, food packaging) (Elsaesser and Howard 2012) or after mucociliary clearance of nanoparticles from the airways (Vega-Villa et al. 2008). Gastrointestinal or oral route is an important route of exposure of nanoparticle-containing drugs. Nanoparticles are efficiently absorbed through the mucosal tissue of the digestive tract and enter into blood and lymphatic circulation (Ramachandran 2011).

3.4 Other route

Intravenous route is a useful route for the studies on the biodistribution and toxicology in the experimental models. Intravenous injection of nanoparticles demonstrated the distribution passage and direct effects of nanopaticles to the systemic organs *in vivo* (Austin et al. 2011; Balasubramaniun et al. 2010; De Jong et al. 2008; Lasagna-Reeves et al. 2010; Sadauskas et al. 2007; Saduaskas et al., 2009a; Semmler-Behnke et al. 2008; Takahashi and Matsuoka 1981; Yamashita et al. 2011). Intravenous route is also important for several medical treatment or diagnosis using nanoscale materials (Austin et al. 2011; Saunders 2009).

4. Translocation of nanoparticles to the systemic circulation and their distribution

For pathological and toxicological studies, the potential hazard nanoparticles are better to examine wheter nanoparticles may access to the systemic circulation and reach the systemic organs (Elsaesser and Howard 2012; Sadauskas et al. 2009a). The major concern is involved in the biological barriers such as the air–blood barrier, the blood–brain barrier, or the maternal–fetal (placental) barrier (Elasesser and Howard, 2012; Saunders, 2009).

The translocation and biodistribution of nanoparticles demonstrated the quite different pattern depending on the administered route (Semmler-Behnke et al. 2008). The translocation of inhaled nanoparticles into the systemic circulation to reach other systemic organs can be

occurred in the air–blood barrier (Naota et al. 2013; Sadauska et al. 2009b; Saunders 2009; Yu et al. 2007), but not a low concentration (Elsaesser and Howard 2012; Semmler-Behnke et al. 2008). Experimentally, nanoparticles can be uptake in alveolar epithelial cells by endocytosis after inhalation exposure and can be detected in the livers of mice after intratracheal instillation (Sadauskas et al. 2009b; Yu et al. 2007). In addition, phagocytosis by alveolar macrophages may be responsible for translocation of nanoparticles through the blood circulation (Furuyama et al. 2009; Yang et al. 2008).

Recent studies demonstrated that nanoparticles could be found in the various tissues including liver, lung, spleen, kidneys, brain, heart, skin, uterus, placentas, embryos, fetuses, including urine and feces after intravenous administration (Austin et al. 2011; Balasubramanian et al. 2010; Lasagna-Reeves et al. 2010; Semmler-Behnke et al. 2008; Yamashita et al. 2011).

5. Nanoparticle Toxicity

Nanoparticles are showing toxicities both *in vivo* and *in vitro* studies and link to the occurrence of several diseases (Figure 2). The parameters for nanoparticles toxicological studies are concentrations, characteristics of particles, and time of exposures (Elsaesser and Howard, 2012). *In vivo* studies described the adverse effects after exposure to several nanoparticles. Subcutaneous injection of titanium dioxide nanoparticles (TiO_2, 25–70 nm in size) induced genital and cranial nerve damage in mice (Chu et al. 2010). Silica dioxide nanoparticles ($nSiO_2$, 70 nm in size) and TiO_2 nanoparticles (35 nm in size) caused the pregnancy complications such as induction of placental structural abnormalities, small fetuses and increased fetal resorption rates after intravenous administration in mice (Yamashita et al. 2011). The intranasal instillation of TiO_2 nanoparticles induced acute pulmonary inflammation in pregnant mice and increased asthma susceptibility in pups (Fedulov et al.

2008). In addition, the intraperitoneal injection of C_{60} fullurenes caused death and induced abnormalities of mouse embryos (Tsuchiya et al. 1996). *In vitro* cytotoxicity of nanoparticles has been carried out in various cell lines. For example, the previous studies suggested that CoCr nanoparticles (29.5 nm in size) induced DNA damage of human trophoblast choriocarcinoma cell line and layer of BeWo b30 cells (Bhaba et al. 2009). TiO_2 nanoparticles (25–70 nm in size) was shown to inhibit the proliferation of mouse testis Leydig cell line TM3 (Komatsu et al. 2008). The studies in mouse germ line stem cells (spermatogonia stem cell line C18-4) also demonstrated that silver nanoparticles (15 nm in size), aluminium nanoparticles (30 nm in size) and MoO_3 nanoparticles (30 nm in size) induced necrosis and apoptosis of cell lines (Bradich-Stolle et al. 2005).

The possible mechanisms on the nanoparticles toxicity can be either chemical or physical mechanisms. Chemical mechanism includes the production of reactive oxygen species (ROS), induction of oxidative damage, releasing of toxic ions, and disturbance of cell functions (Elasesser and Howard 2012). Physical mechanism includes the impairment of cell membrane structures, cell membrane activities, transport processes and protein activities of the cells (Chen and von Mikecz 2005). Moreover, nanoparticles are capable to interact directly with DNA, which can cause DNA damage and potentially induce genotoxicity (Bhabra et al. 2009; Mehrabi and Wilson 2007).

6. Exposure to nanoparticles during specific conditions

6.1 Co-exposure of nanaoparticles and ambient particulate matter (PM)

Ambient particulate matter (PM) consisting of mainly airborne particulate matter represents the term used for a complex mixture of organic and inorganic substance. Several ambient PMs originate from nature such as volcanoes, dust storms, grassland fires and from human activities such as the combustion of fuels in vehicles, power plants and various

industrial processes (Bell and Davis 2001; European commission 1997). The composition of PMs depends on their sources. PM can be classified into the primary particles, particles are which released directly into the environment from the source of generation, and the secondary particles, particles that are formed in the atmosphere through gas-to-particle conversion (European Commission 1997). In addition, PM can be classified by their physical sizes, e.g. ultrafine particles ($PM_{0.1}$), fine particles ($PM_{2.5}$), and coarse particles (PM_{10}) (WHO 2003).

Over the past two decades, numerous epidemiological studies have shown that the exposure to ambient particulate matter (PM) increases the risk of death and health problems in both developed and developing countries (Li et al. 2008; Nemmar et al. 2010; WHO 2005). World Health Organization (WHO) also indicated the relation between ambient PM exposure and the hospitalization for the various diseases, such as, chronic cardiopulmonary diseases, asthma and atherosclerosis (WHO 2003).

6.1.a Asian sand dust

Asian sand dust is one of ambient airborne PM. Asian sand dust originates from the Gobi desert and Loess plateau of China and Mongolia (Kim et al. 2010; Park et al. 2010). During the winter and spring seasons, dust storms spread and transport dust particles to far-reaching areas such as China, Mongolia (Park et al. 2010), South Korea (Chung and Yoon 1996; Kim et al. 2010), Taiwan (Chen et al. 2004; Chang et al. 2010), Japan (Mori et al. 2003; Maki et al. 2010), the United States and Canada (Husar et al. 2001; Tratt et al. 2001; Zdanowicz et al. 2006). Asian sand dust commonly consists of rock-forming minerals, e.g. quartz and feldspar, and clay forming minerals, e.g. mica, kaolinite and chlorite (Nishikawa et al. 2000). Recently, frequency and intensity of Asian sand dust phenomena have been increasing because of global climate change (Hiyoshi et al. 2005; Ichinose et al. 2005; Naota

et al. 2010). For those reasons, the concern about Asian sand dust phenomenon and its effect also increased.

6.1.b Health effect related to Asian sand dust exposure

Epidemiologic studies have shown that Asian dust affects human health in several regions (Figure 3). A concomitant increase in respiratory and cardiovascular problems has been reported in Taiwan (Yang et al. 2005), China (Meng and Lu 2007), and Korea (Hong et al. 2010). In experimental animal models, exposure to Asian sand particles induced an acute neutrophilic inflammation in bronchi and alveoli (Ichinose et al. 2005; Naota et al. 2010) and exacerbated allergic alveolitis with goblet cell proliferation in the airways (Hiyoshi et al. 2005). Intratracheal instillation of Asian sand particles also induced inflammatory cell proliferation and increased the level of bronchoalveolar lavage fluid (BALF) chemokines and inflammatory cytokines (Ichinose et al. 2005; Naota et al. 2010). Exposure to Asian sand dust results in acute pulmonary injury (Ichinose et al. 2005; Naota et al. 2010), and it may enhance the translocation of nanoparticles into the systemic circulation across the damaged air–blood barrier, thereby exacerbating systemic toxicity (Figure 4) (Saunders 2009). There are, however, no reports of the effects of exposure to nanoparticles in an injured pulmonary condition .

6.2 Exposure during pregnancy

Humans are known to be sensitive to toxic materials during pregnancy, especially fetuses in the pre-natal stages (Kulvietis et al. 2011; Yamashita et al. 2011). Several reports indicated an increased perinatal mortality, pre-term birth and birth defects correlated with particulate matter exposure during pregnancy (Buerki-Thurnherr et al. 2012; Ema et al. 2010). As metioned above, the risk of exposure to nanoparticles in pregnancy increases, the placental transfer of nanoparticles has become of great concern in assessing the safety of nanoparticles in pregnancy for the associated risk of growth and developmental defects in the fetuses

(Buerki-Thurnherr et al. 2012; Cartwright et al. 2012; Saunders 2009; Yamashita et al. 2011). In mammals, the potential fetal toxicity depends on the translocation of particles from the maternal circulation, which is mainly determined by the maternal–fetal barrier (Kulvietis et al. 2011). The placenta is the organ that connects the maternal and fetal circulation. Oxygen and nutrient exchanges between the mother and fetus occur in the maternal–fetal barrier at the labyrinthine zone of the placenta (Bureki-Thurnherr et al. 2012; Furukawa et al. 2011; Khan et al. 2011; Takata et al. 1997). In addition, toxic substances can also transfer across the maternal–fetal barrier. Accordingly, placenta is a critical site for fetal intoxication (Ema et al. 2010; Keelan 2011; Saunders 2009). The murine placenta like the human placenta is that the maternal and fetal circulations are separated by the endothelium and trophoblasts (Furukawa et al. 2011; Kirby and Bradbury 1965; Khan et al 2011). Although there are some differences such as the number of trophoblast layers between maternal and fetal circulations. However, the placentas of human and murine have strong similarities (Cox et al. 2009). Therefore, murine placental model is commonly used for many researches (Keelan 2011; Yamashita et al 2011).

Several mechanisms are already known for the placental exchange of endogenous substances including passive diffusion, facilitated diffusion, putative transtrophoblast channel, and active transport (Buerki-Thurnherr et al. 2012; Kulvietis et al 2011). Macropinocytosis, classical clathrin-dependent, non-classical clathrin-independent (caveolae-dependent) or clathrin- and caveolae-independent endocytosis are further proposed as subtypes of endocytosis (Conner and Schmid 2003; Le Roy and Wrana 2005; McMahon and Boucrot 2011; Myllynen et al. 2008). Clathrin, a major protein of clathrin-coated endocytic vesicles, and caveolin-1, a major protein of the caveolae structure (Mohanty et al. 2010), are expressed in trophoblasts and endothelial cells of the rodent placenta during physiological condition

(Figure 5). However, information about the translocation of nanoparticles in the placental tissue during nanoparticle exposure remains unclear.

For these reasons, the present thesis interested in the possible translocation pathway of nanoparticles in the specific conditions, including the pathological condition of lungs induced by Asian sand dust and the maternal–fetal transfer of nanoparticles during pregnancy.

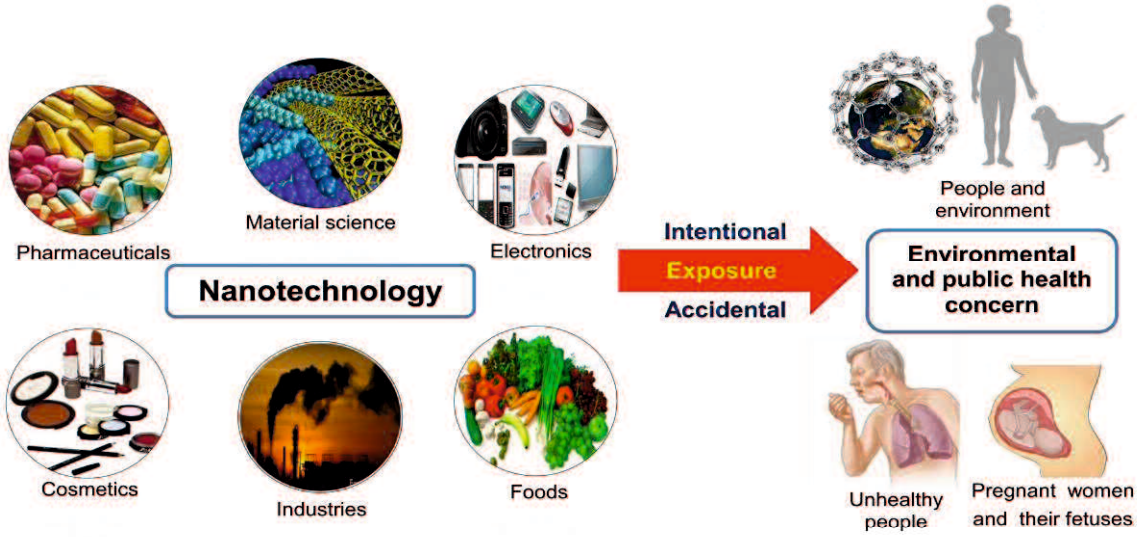

Figure 1. Schematic diagram shows the applications of nanotechnology and the risk of the exposure of nanoparticles to people and environment.

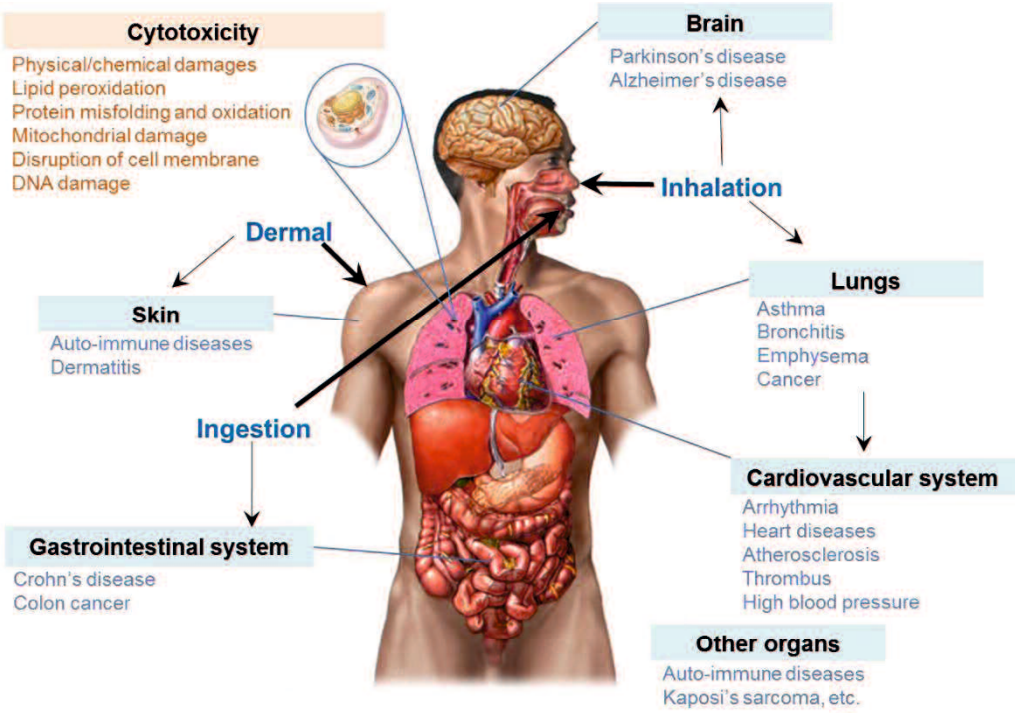

Figure 2. Schematic diagram shows the routes of exposure to nanoparticles and the toxicity of nanoparticles. Several systemic diseases link to the exposure to nanoparticles.

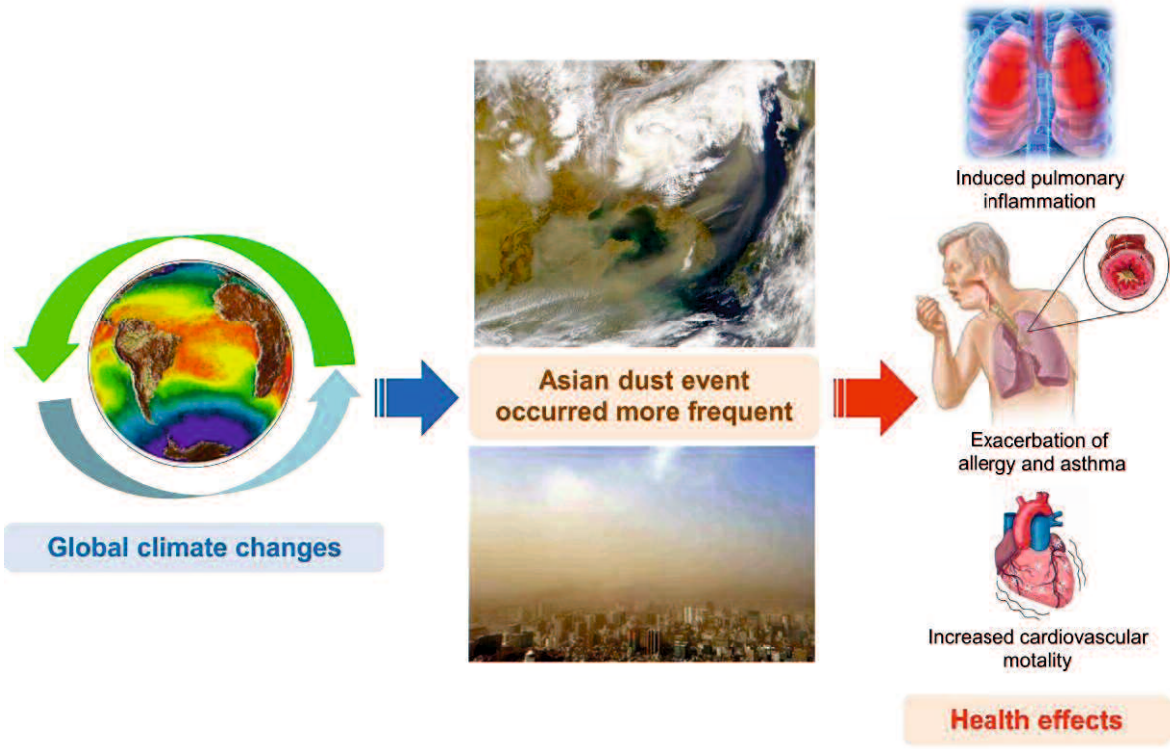

Figure 3. Schematic diagram shows the relationship between Asian sand dust event and the potential adverse health effects. Frequency and intensity of Asian sand dust phenomena have been increasing because of the global climate changes. The exposure of Asian sand dust induces pulmonary inflammation, exacerbates allergy and asthma, and increases cardiovascular mortality and hospitality.

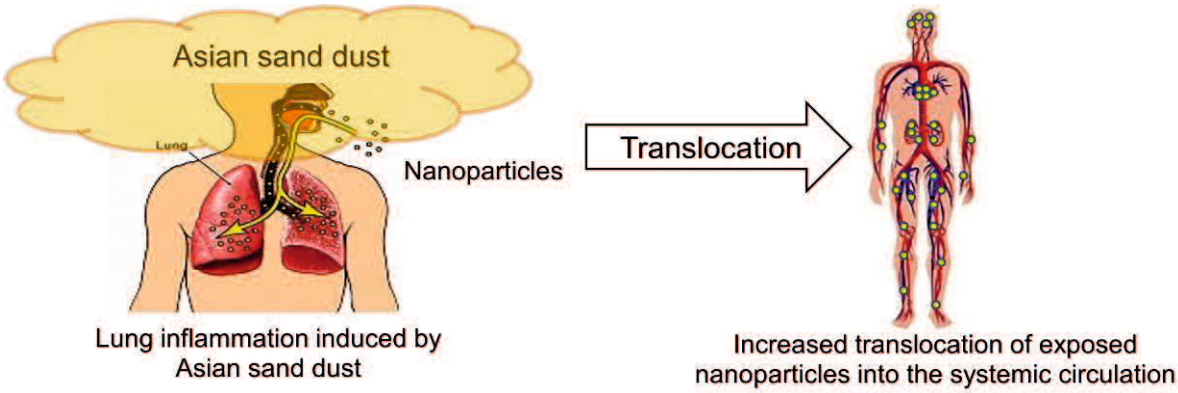

Figure 4. Schematic diagram shows a hypothesis for the risk of the co-exposure of Asian sand dust and nanoparticles. Asian sand dust induces severe acute lung inflammation with a significant injury of the structure of the air–blood barrier. The damage may increase the translocation of the co-exposed nanoparticles into the systemic circulation across the injured air–blood barrier.

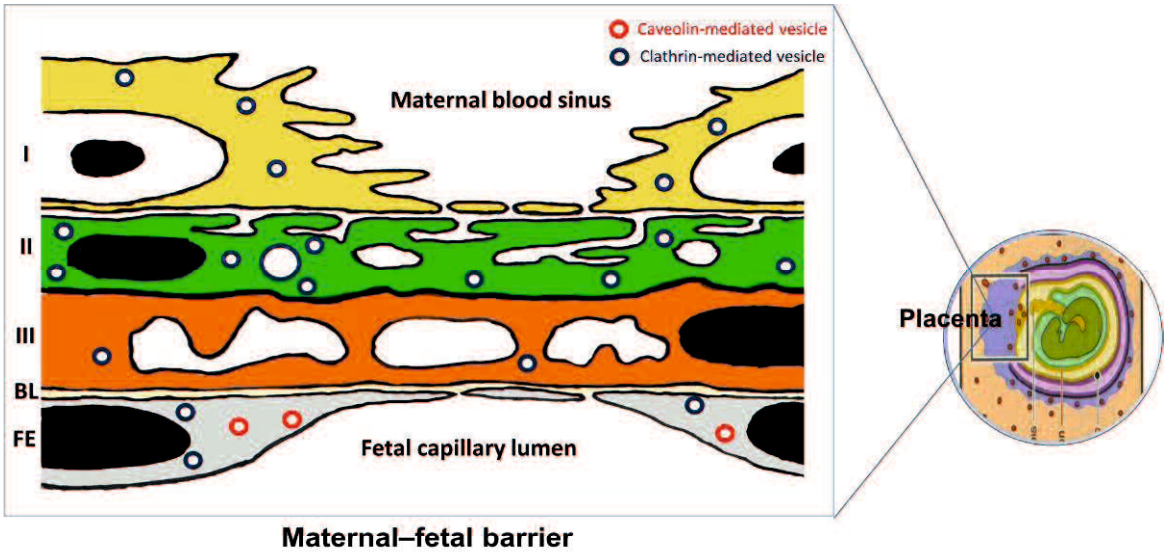

Figure 5. Schematic diagram shows clathrin- and caveolin-mediated endocytosis at the maternal–fetal barrier in rodent placenta in the physiological condition. I = syncytiotrophoblast layer I, II = syncytiotrophoblast layer II, III = syncytiotrophoblast layer III, BL = basal lamina, FE = fetal endothelial cell.

OBJECTIVE AND STRUCTURE OF THE THESIS

The overall objective of this thesis was to determine the possible translocation pathway and the pathological changes after exposure to nanoparticles in the specific conditions including the pathological condition induced by Asian sand dust in lung and the possible translocation pathway and toxicity of nanoparticles in placenta and fetus during pregnancy in mice.

In chapter 1: The specific objective was to investigate a possible translocation pathway of intratracheally instilled gold nanoparticles after induction of acute pulmonary injury by Asian sand dust

In chapter 2: The specific objective was to investigate the possible translocation pathway of gold nanoparticles across the maternal–fetal barrier as well as the toxicity of intravenously administered gold nanoparticles to the placenta and fetus, including clathrin- and caveolin-mediated endocytosis.

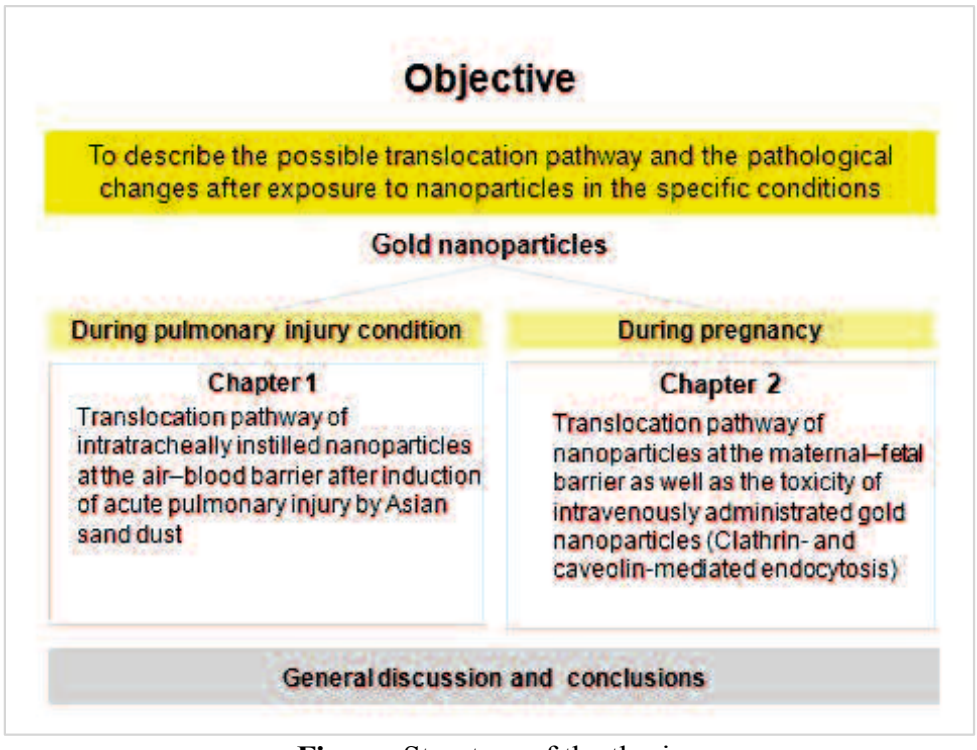

Figure. Structure of the thesis

LIST OF ORIGINAL PUBLICATIONS

The thesis is based on the following original publications.

Rattanapinyopituk, K., Shimada, A., Morita, T., Togawa, M., Hasegawa, T., Seko, Y., Inoue, K., and Takano, H. (2013). Ultrastructural changes in the air–blood barrier in mice after intratracheal instillations of Asian sand dust and gold nanoparticles. *Exp Toxicol Pathol* **65**, 1043–51.

Rattanapinyopituk, K. Shimada, A. Mortia, T. Sakurai, M., Asano, A., Hasegawa, T., Inoue, K., and Takano, H. (2013). Demonstration of clathrin- and caveolin-mediated endocytosis at the maternal–fetal barrier after intravenous administration of gold nanoparticles in mouse placenta. *J Vet Med Sci* In press.

CHAPTER 1

Ultrastructural Changes in the Air–Blood Barrier in Mice after Intratracheal Instillations of Asian Sand Dust and Gold Nanoparticles

ABSTRACT

The purpose of this study was to investigate a possible translocation pathway of intratracheally instilled gold nanoparticles after the induction of acute pulmonary injury by Asian sand dust. ICR mice were intratracheally instilled with 800 μg Asian sand particles (CJ-2 particles) 24 hr before instillation of 50-nm gold nanoparticles. Lungs from mice treated with Asian sand particles and gold nanoparticles showed an acute focal inflammation with an increased expression of proinflammatory cytokines (IL-6 and TNF-α) and oxidative stress markers (Cu/Zn SOD and iNOS) in alveolar macrophages, type I alveolar epithelial cells, and endothelial cells at the alveolar walls. Electron microscopy revealed a destruction of the alveolar walls with an increased number of endocytic vesicles in the cytoplasm of both type I epithelial cells and endothelial cells; gold nanoparticles were demonstrated in these endocytic vesicles. These findings suggest that translocation of the exposed nanoparticles may be enhanced in the lung tissues with acute inflammatory changes.

INTRODUCTION

Asian sand dust originates from the Gobi desert and Loess plateau of China and Mongolia (Kim et al. 2010; Park et al. 2010). During the winter and spring seasons, dust storms spread and transport dust particles to far-reaching areas such as China, Mongolia (Park et al. 2010), South Korea (Chung and Yoon 1996; Kim et al. 2010), Taiwan (Chen et al. 2004; Chang et al. 2010), Japan (Mori et al. 2003; Maki et al. 2010), the United States, and Canada (Husar et al. 2001; Tratt et al. 2001; Zdanowicz et al. 2006). Epidemiologic studies have shown that Asian dust affects human health in several regions. A concomitant increase in respiratory and cardiovascular problems has been reported in Taiwan (Yang et al. 2005), China (Meng and Lu 2007), and Korea (Hong et al. 2010). In experimental animal models, exposure to Asian sand particles induces an acute neutrophilic inflammation in bronchiole and alveoli (Ichinose et al. 2005; Naota et al. 2010) and exacerbates allergic alveolitis with goblet cell proliferation in the airways (Hiyoshi et al. 2005). Intratracheal instillation of Asian sand particles also induces inflammatory cell proliferation and increases the level of bronchoalveolar lavage fluid (BALF) chemokines and inflammatory cytokines (Ichinose et al. 2005; Naota et al. 2010). In a normal environment, ambient air is a mixture of various types of materials (Inoue et al. 2007; Laks et al. 2008). On a daily basis, people are exposed to many kinds of substances, either on purpose or accidentally. Nanotechnology is developing rapidly and is involved in a wide range of applications. Therefore, the exposure to nanoscale materials and their potential toxicity are of great concern. Gold nanoparticles are well-known nanomaterials with multipurpose usages (Balasubramanian et al. 2010; De Jong et al. 2008; Sadauskas et al. 2009a). A number of studies have demonstrated that the translocation of gold nanoparticles into the systemic circulation is extremely low after intratracheal instillation and inhalation in physiological conditions (Lipka et al. 2010; Sadauskas et al. 2009a; Semmler-

Behnke et al. 2008; Takenaka et al. 2006; Yu et al. 2007). Seasonal or daily exposure to endemic or epidemic pollutants such as Asian sand dust results in acute pulmonary injury (Ichinose et al. 2005; Naota et al. 2010), and it may enhance the translocation of nanoparticles into the systemic circulation across the damaged air–blood barrier, thereby exacerbating systemic toxicity. Several reports have described the effects and the translocation process of gold nanoparticles after intratracheal instillation in healthy mice (Furuyama et al. 2009; Sadauskas et al. 2009a). There are, however, no reports of the effects of exposure to gold nanoparticles in an injured pulmonary condition. The purpose of this study was to investigate the possible translocation pathway of 50-nm gold nanoparticles in the pulmonary pathological condition induced by Asian sand dust in mice.

MATERIALS AND METHODS

Animals

Fifty-five male ICR mice (7 weeks old, 33–36 g) were obtained from CLEA Japan Inc. (Tokyo, Japan). Commercial diet CE-2 (CLEA Japan Inc.) and tap water were given *ad libitum* throughout the experiment. Mice were housed at approximately 25°C, in 55–70% relative humidity, and in a 12-hr light/dark cycle. All animal experiments were conducted according to the Tottori University guidelines for animal welfare.

Particle preparation

Preparation and morphology of Asian sand particles

Simulated Asian mineral dust (CJ-2 particles) collected from Tengger Desert, China, was purchased from General Sciences Cooperation (Tokyo, Japan). The primary mineral component was composed of 28.0% Si, 5.9% Al, 5.3% Ca, and 3.0% Fe (according to the manufacturer's data sheet). A morphological examination of the CJ-2 particles was performed with a scanning electron microscope (SEM Model X-650, Hitachi, Tokyo, Japan). The particles were pleomorphic and had rough surfaces (Figure 1A).

Preparation and morphology of gold nanoparticles

A 0.01% 50-nm colloidal gold solution (mean diameter, 49.3 nm; BB International, Cardiff, UK) was concentrated into a 0.1% solution by centrifugation. After centrifugation, the sediment pellets were suspended in normal saline solution. A morphological examination

of the colloidal gold suspension under transmission electron microscopy (TEM-100CX, Japan Electron Optical Laboratory, Tokyo, Japan) showed electron-dense, spherical, uniform, and individual or slightly agglomerated particles (Figure 1B).

Experimental protocol

ICR mice were divided into 2 treated groups and 1 control group. All mice were anesthetized by intraperitoneal administration of sodium pentobarbital (5 mg/100 g body weight) before particle treatment. All mice were intratracheally instilled with 0.05 ml of solution, followed by 0.15 ml of air, with a small cannula. The suspensions were agitated immediately before instillation.

Mice were first intratracheally instilled with 800 μg CJ-2 particles (CJ-2 particles and gold nanoparticles treated group, n = 20) or normal saline (gold nanoparticles treated group, n = 20). After 24 hr, mice were instilled a second time with a 0.1% 50-nm colloidal gold solution. The control mice (n = 15) were instilled with 0.05 ml of saline solution on both occasions (Figure 2).

Lungs and other organ samples

Eight mice from each of the treated groups and 6 mice from the control group were sacrificed by exsanguination under deep anesthesia induced by an intraperitoneal injection of sodium pentobarbital. At 5 min after the second instillation, the lungs were collected for histopathology, immunohistochemistry, autometallography (AMG), and transmission electron microscopy. Four mice from the treated groups and 3 mice from the control group were used for BALF collection.

At 1 hr after the second instillation, mice from the treated groups (n = 8 per group) and the control group (n = 6) were sacrificed, and various organs (lungs, liver, kidneys, spleen, heart and brain) were collected for histopathologic, autometallographic examinations, and inductively coupled plasma–mass spectroscopy (ICP-MS).

Histopathology

Lungs were fixed by infusion and immersion in 10% neutral-buffered formalin. Other tissues (liver, kidney, spleen, heart, and brain) were fixed by immersion in 10% neutral-buffered formalin. Formalin-fixed tissues were processed using routine pathological methods and embedded in paraffin blocks. Tissue sections (3-μm-thick) were cut for hematoxylin and eosin staining, immunohistochemistry, and AMG. A lung score was determined by scoring the degree of bronchiolar and alveolar inflammation (Table 1, modified from Naota et al. 2010). The histopathological examination was performed by 2 pathologists in a blind manner.

Immunohistochemistry

Paraffin-embedded thin sections of the lungs of mice from the treated groups (n = 8) and the control group (n = 6) were used for immunohistochemical detection of laminin, interleukin (IL)-6, tumor necrosis factor (TNF)-α, dimeric copper- and zinc-containing superoxide dismutase (Cu/Zn SOD), and inducible nitric oxide synthase (iNOS). For antigen retrieval, the sections were treated with proteinase K (Dako, Denmark) for 30 min (for laminin detection) or placed in citrate buffer (pH 5.4) and microwaved (for the detection of IL-6, TNF-α, Cu/Zn SOD, and iNOS). Endogenous peroxidase activity was quenched with 3% H_2O_2 at room temperature for 30 min. The slides were then blocked with 10% normal

goat serum (laminin, TNF-α, and iNOS) or 10% bovine serum albumin (IL-6) for 5 min in a microwave. Next, sections were incubated with primary antibodies at 4°C overnight (anti-laminin: Dako, Denmark, 1:1,000 dilution; anti-IL-6: Santa Cruz Biotechnology, Santa Cruz, CA, 1:200 dilution; TNF-α: Monosan, Uden, the Netherlands, 1:15 dilution; anti-Cu/Zn SOD: Stressgen Bioreagents, Victoria, Canada, 1:200 dilution; and anti-iNOS: BD Transduction Laboratories, Lexington, KY, 1:125 dilution) or an equivalent amount of phosphate-buffered saline as a negative control. Lung sections from mice intratracheally instilled with CJ-2 particles were used as positive control for immunohistochemistry (Naota et al. 2010). A labeled streptavidin biotin kit (Dako, Denmark) was used to detect immunoreaction complexes in the avidin–biotin complex assay. Positive immunoreactions appeared as brown staining with 3,3′-diaminobenzidine tetrahydrochloride (DAB). Sections were counterstained with hematoxylin and observed by light microscopy. IL-6- and TNF-α positive cells were counted in 4 randomly selected lesions at ×100 magnification.

Autometallography

Paraffin sections of lungs, livers, kidneys, spleen, heart and brain tissues were used for the AMG analysis (Danscher 1984; Danscher and Stoltenberg 2006). The sections were developed in a physical developer consisting of 50% gum arabic, 50% citrate buffer, 5.6% hydroquinone, and 17% silver nitrate. The reaction was conducted in a water bath at 26°C for 1 hr in the dark. The excessive silver residue was removed with a 5% sodium thiosulfate solution for 10 min. Next, sections were counterstained with hematoxylin. The invisible gold nanoparticles deposited in the tissue were visualized by a surrounding shell of small black silver grains.

Electron microscopy

Four mice from each group were sacrificed 5 min after the second instillation. Half of the longitudinal sections from each lobe of the lung were cut into cubes measuring 1–2 mm^3. Next, tissues were fixed in glutaraldehyde for 3 hr at 4°C, rinsed in 0.1 M phosphate buffer (pH 7.4), post-fixed with 1% osmium tetroxide for 1 hr, dehydrated in alcohol, and embedded in epoxy resin. The areas of interest were selected for electron microscopic examination from 1% toluidine-stained semi-thin (1-μm-thick) sections and subsequently cut into ultra-thin (70-nm-thick) sections (Naota et al. 2010). After staining with uranyl acetate and lead citrate, ultra-thin sections were examined by TEM-100CX electron microscope.

BALF analysis

The BALF collected from the lungs after the second intratracheal instillation was used for the cellular analysis. Briefly, 37°C normal saline was used as the lavage fluid. Each 0.12-ml volume of lavage fluid was gently aspirated and harvested from the lungs via a tracheal cannula after euthanasia. Three lavage fluids were combined, cooled down to 4°C, and then centrifuged at 3,000 rpm for 10 min. Cell pellets were used for determining the total cell number, cell viability, and differential cell count. A total of 200 cells were counted by light microscopy (Naota et al. 2010).

Inductively coupled plasma–mass spectroscopy (ICP-MS)

Tissue gold concentration was analyzed according to the method of Sonavane et al. (2008). 0.1 g of tissues (lung, liver, kidney, spleen, heart, and brain) from mice of the treated

groups (n = 4) and control group (n = 3) were digested with 2 ml of aqua regia. After digestion, the inorganic residues were dissolved in 5 ml of 0.05 N HCl, ultrasonicated for 20 min, and the samples were analyzed by inductively coupled plasma–mass spectroscopy (ICP-MS) (HP 4500, Agilent Technologies). The detection and quantification limits for gold were 0.5 ng/ml and 1 ng/ml, respectively.

Statistical analysis

All data were expressed as the mean ± standard error (S.E.). Statistical significance was determined by a Student's t-test for two-group comparisons. For all comparisons, P values less than 5% ($P < 0.05$) were considered statistically significant.

RESULTS

Histopathology

The control mice showed no pathological changes in lung tissues. Lungs from mice instilled with gold nanoparticles alone showed a mild thickening of the alveolar walls with increased activated macrophages and mild alveolitis (Figure 3A), but the average lung score was not significantly different from the lung score of the control mice (Table 2). Lungs from mice instilled with CJ-2 particles and gold nanoparticles demonstrated a multifocal deposition of CJ-2 particles in the bronchiolar and alveolar spaces (Figure 3B). The alveolar walls were thickened by an infiltration of neutrophils and alveolar macrophages (Figure 3B). Degenerative changes of the alveolar walls were occasionally observed, predominantly in areas adjacent to the CJ-2 particles (Figure 3C). Lungs from mice treated with CJ-2 particles and gold nanoparticles showed the highest average lung score with statistical significance (Table 2).

No pathological lesions were found in the other organs from the mice treated with gold nanoparticles alone, the mice treated with CJ-2 particles and gold nanoparticles and control mice.

Electron microscopy

The lungs collected from mice intratracheally instilled with gold nanoparticles alone and from mice instilled with CJ-2 particles and gold nanoparticles demonstrated an increase in the number of endocytic vesicles in the cytoplasm of type I alveolar epithelial cells and endothelial cells (Figures 4B–D) compared to the control (Figure 4A). A ruffling of the

surface of type I epithelial cells was also observed in lungs of the mice instilled with gold nanoparticles alone (Figure 4C). Lungs from the mice instilled with CJ-2 particles and gold nanoparticles showed a swelling of type I alveolar epithelial cells (Figure 4D). Degeneration and detachment of the type I epithelial cell with edematous swelling were occasionally observed (Figure 5). Gold nanoparticles were seen attached to the surface of type I alveolar epithelial cells (Figures 6A and 6B) and were found in the endocytic vesicles (Figure 6B) in the cytoplasm of type I epithelial cells from mice instilled with gold nanoparticles alone and from the mice instilled with CJ-2 particles and gold nanoparticles.

Immunohistochemistry

Laminin immunohistochemistry revealed 2 continuous layers of strong positivity in the basement membrane of the alveolar walls in the control mice. This finding was similar the changes of lungs from the mice instilled with gold nanoparticles alone (Figure 7A). Lungs from mice instilled with CJ-2 particles and gold nanoparticles showed markedly discontinuous and unclear basement membranes particularly at the areas adjacent to the foci of infiltrated inflammatory cells (Figure 7B).

IL-6 and TNF-α expression was detected in the cytoplasm of alveolar macrophages, with a weak expression found in type I and II alveolar epithelial cells (Figure 8 and Figure 9). The number of both IL-6– and TNF-α–positive alveolar macrophages in the lungs from the mice instilled with CJ-2 particles and gold nanoparticles was significantly greater than that from the mice instilled with gold nanoparticles alone (Table 3). The control mice showed less positive immunolabeling compared to the treated groups (Figure 8A and Figure 9A).

Cu/Zn SOD immunohistochemistry showed a positive expression in alveolar macrophages and a weak expression in neutrophils and type I and II alveolar epithelial cells

(Figure 10). The intensity of the immunolabeling was the highest in the mice instilled with CJ-2 particles and gold nanoparticles (Figure 10C). Lungs from the mice instilled with gold nanoparticles alone demonstrated less immunopositivity in alveolar macrophages and type I alveolar epithelial cells (Figure 10B). iNOS immunohistochemistry showed an intense in positive expression in alveolar macrophages, and type I and type II alveolar epithelial cells in the mice instilled with CJ-2 particles and gold nanoparticles (Figure 11C). Lungs from the mice instilled with gold nanoparticles alone showed less immunopositivity (Figure 11B). Control lungs showed the least immunolabeling for Cu/Zn SOD and iNOS (Figure 10A and Figure 11A).

BALF analysis

The number of alveolar macrophages significantly increased in the BALF collected from lungs of the mice instilled with gold nanoparticles and the mice instilled with CJ-2 particles and gold nanoparticles compared to the control, whereas the neutrophil number significantly increased only in the BALF from the mice instilled with CJ-2 particles and gold nanoparticles (Table 4). The cell viability of treated groups was not significantly different from that of the control (Table 4).

Autometallography

Silver-enhanced gold nanoparticles were detected in the lungs of the mice instilled with gold nanoparticles and mice instilled with CJ-2 particles and gold nanoparticles. At 5 min after the instillation of gold nanoparticles, the particles were observed in alveolar macrophages and occasionally on the surface of the alveolar lumens (Figure 12A and Figure

12B). Gold nanoparticles were not detected by the AMG method in other organs from any of the treated groups.

ICP-MS

Gold content was detected only in the lungs from the mice instilled with gold nanoparticles alone and mice instilled with CJ-2 particles and gold nanoparticles.

DISCUSSION

Seasonal Asian sand dust (Kosa) causes serious environmental and public health problems in many countries (Meng and Lu 2007; Hong et al. 2010; Yang et al. 2005). Asian sand particles can cause a respiratory tract inflammation in mice after intratracheal instillation (Hiyoshi et al. 2005; Ichinose at al. 2005; Naota et al. 2010). The exposure to nanoparticles during pulmonary inflammation is a concern because nanoparticles may easily translocate into the systemic circulation and induce adverse effects (Nemmar et al. 2010; Sadauskas et al. 2009a; Saunders 2009). This study aimed to investigate a possible translocation pathway of intratracheally instilled gold nanoparticles in acute pulmonary injury induced by Asian sand dust in mice.

In the present study, an instillation of Asian sand particles and gold nanoparticles induced severe acute inflammatory changes in lung tissue. Instilled lungs showed a multifocal infiltration of neutrophils and macrophages with a destruction of the alveolar walls. In contrast, mice treated with gold nanoparticles alone showed only a mild thickening of alveolar walls with an increase in the number of activated macrophages. Laminin immunohistochemistry was performed to demonstrate the injurious changes in the alveolar walls. Lungs from mice treated with Asian sand particles and gold nanoparticles showed a discontinuous and light immunolabeling of laminin in the alveolar walls. Laminin is an important component of the alveolar wall, supporting its cellular attachments and its stability (Aumailley and Smyth 1998; Naota et al. 2010). Therefore, laminin immunolabeling has been used as an indicator of alveolar wall destruction (Kaewamatawong et al. 2005; Naota et al. 2010). Ultrastructural findings of lungs from the mice treated with Asian sand particles and gold nanoparticles also showed severe injury to the alveolar wall structure. Detachment and degeneration of type I epithelial cells, alveolar interstitial edema were observed in contrast to

lungs from the mice treated with gold nanoparticles alone. These findings suggest that Asian sand particles may have severe toxic effects on the structure of the air–blood barrier. An intense expression of proinflammatory cytokines, including IL-6 and TNF-α, and oxidative stress markers, including Cu/Zn SOD and iNOS, was found in alveolar macrophages, type I and II alveolar epithelial cells, and endothelial cells at the alveolar walls of lungs from the mice instilled with Asian sand particles and gold nanoparticles. In the present study, histological and BALF analysis demonstrated markedly increased numbers of neutrophils in lungs instilled with Asian sand and gold nanoparticles. Expression of IL-6 and TNF-α observed in the lung lesions in this study may be responsible for the inflammatory changes dominated by neutrophils (Cho et al. 2007; Hiyoshi et al. 2005; Ichinose et al. 2005). Ultrafine silica particles are known to induce production and release of numerous proinflammatory cytokines, such as IL-1β, IL-6, and TNF-α, which regulate the pulmonary inflammatory process by further release of chemoattractant proteins capable for migration of neutrophils (Cho et al. 2007; Hiyoshi et al. 2005; Ichinose et al. 2005; Naota et al. 2010). From the results, the release of proinflammatory cytokines and the generation of oxidative stress may be involved in the pulmonary destruction induced by Asian sand particles (Hamilton et al. 2008; Ichinose et al. 2005; Meng and Zhang 2006; Naota et al. 2010).

An increased number of endocytic vesicles containing gold nanoparticles was found in the alveolar epithelial cells and in the endothelial cells following inhalation and intratracheal instillation of various sizes of gold nanoparticles in rodents (Furuyama et al. 2009; Takenaka et al. 2006). Endocytosis was shown to play an important role in the internalization of many ultrafine particles, including titanium dioxide nanoparticles (Singh et al. 2007), carbon black nanoparticles (Hussain et al. 2009; Shimada et al. 2006; Inoue et al. 2009), and gold nanoparticles (Shukla et al. 2005). In this study, electron microscopy demonstrated a ruffling of the surface of type I epithelial cells and an increase in the number

of endocytic vesicles in both type I alveolar epithelial cells and endothelial cells at the alveolar wall of both lungs from the mice treated with gold nanoparticles alone and lungs from the mice treated with Asian sand particles and gold nanoparticles. At 5 min after the instillation of gold nanoparticles, attachment of the particles to the surface of alveolar epithelial cells and the presence of the particles inside the endocytic vesicles were observed. These findings suggest that translocation of the exposed nanoparticles may be enhanced in the lung tissues with acute inflammatory changes (Inoue et al. 2009; Saduaskas et al. 2009a; Saunders 2009). In addition, by AMG analysis, gold nanoparticles were also found in alveolar macrophages and on the surface of the alveolar lumen in both lungs from the mice treated with gold nanoparticles alone and lungs from the mice treated with Asian sand particles and gold nanoparticles. Positive AMG findings were dominant in alveolar macrophages, suggesting that alveolar macrophages may take up and eliminate nanoparticles from the alveoli through a phagocytic process (Furuyama et al. 2009; Saunders 2009; Takenaka et al. 2006; Yang et al. 2008).

No gross or histopathological lesions were observed in the systemic organs from the mice treated with Asian sand particles and gold nanoparticles or the mice treated with gold nanoparticles alone. An AMG and gold content analysis by ICP-MS also showed no signs of translocation of gold nanoparticles into other organs except the lungs, suggesting that very low amounts of gold nanoparticles may translocate into the systemic circulation (Sadauskas et al. 2009a; Sadauskas et al. 2009b; Semmler-Behnke et al. 2008; Yu et al. 2007) and that the sensitivity for the detection of gold nanoparticles will be limited to investigate due to the small numbers of gold nanoparticles in the systemic organs (Bettmer et al. 2009; Danscher and Stoltenberg 2006). In addition, the time of tissue sampling following treatment might be one of the factors influencing the results in this study. Previous reports have demonstrated gold nanoparticles in the lungs, as well as in systemic organs at 2 hr after inhalation in mice

(Yu et al. 2007), while samples in the present study were collected only 1 hr after instillation of gold nanoparticles.

In conclusion, Asian sand dust induced severe acute lung inflammation with a significant degeneration of the structure of the air–blood barrier. The damage may increase the risk of translocation of the co-exposed nanoparticles into the systemic circulation.

FIGURES AND FIGURE LEGENDS

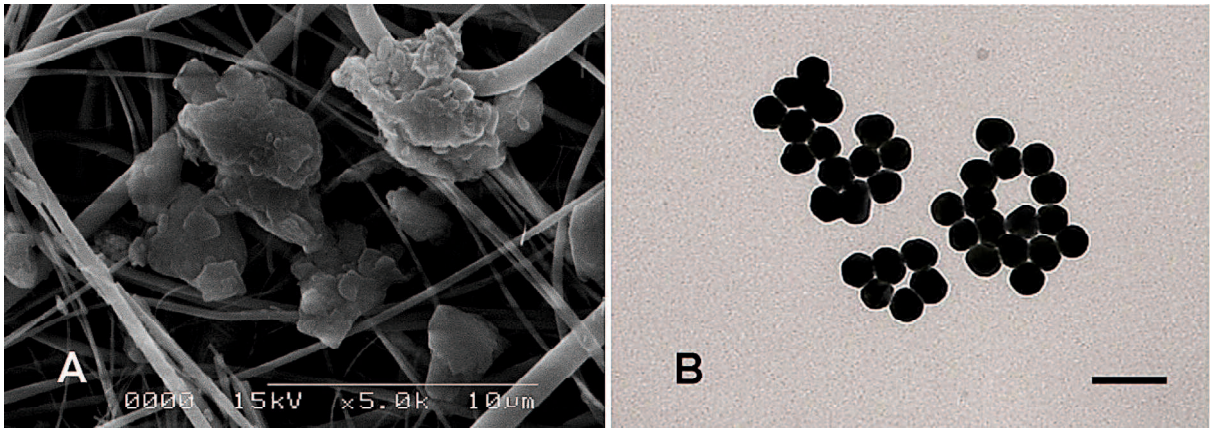

Figure 1. Morphological findings of particles. (A) CJ-2 particles show pleomorphism with rough surfaces under scanning electron microscopy. Bar = 10 μm. (B) Transmission electron micrograph of 50-nm gold nanoparticles shows electron-dense, spherical, and uniform appearance. Bar = 100 nm.

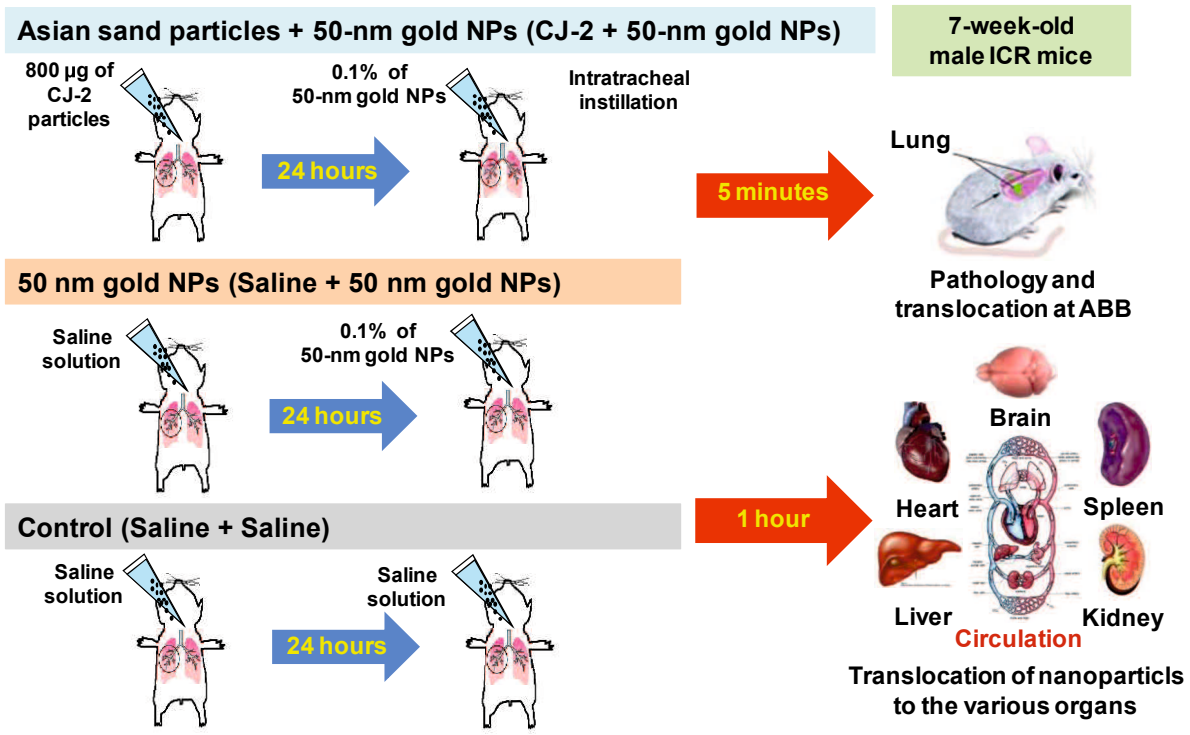

Figure 2. Schematic diagram shows the materials and methods of the experiment. Seven-week-old male ICR mice were divided into 2 treatment groups and 1 control group. Mice were first intratracheally instilled with 800 μg CJ-2 particles (CJ-2 particles and gold nanoparticles treated group) or normal saline (gold nanoparticles treated group). After 24 hr, mice were instilled a second time with a 0.1% 50-nm colloidal gold solution. The control mice were instilled with 0.05 ml of saline solution on both occasions. At 5 min after the second instillation, the lungs were collected for histopathology, immunohistochemistry, autometallography (AMG), and transmission electron microscopy. Four mice from the treated groups and 3 mice from the control group were used for BALF collection. At 1 hr after the second instillation, various organs (lungs, liver, kidneys, spleen, heart, and brain) were collected for histopathologic, autometallographic examinations, and inductively coupled plasma-mass spectroscopy (ICP-MS). ABB = air–blood barrier

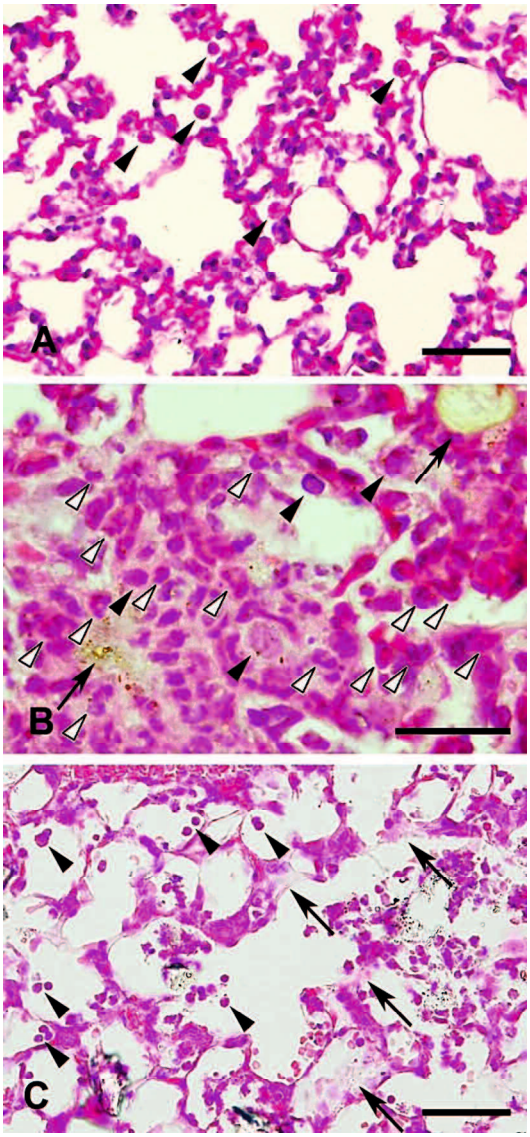

Figure 3. Lung lesions of the mice following intratracheal instillation of particles. Lung from the mice instilled with 50-nm gold nanoparticles alone shows mild thickening of alveolar walls with increase in the number of activated macrophages (arrowheads) (A). Bar = 50 μm. Lung from the mice instilled with 800 μg of CJ-2 particles and 50-nm gold nanoparticles shows focal infiltration of neutrophils (white solid arrows) and activated macrophages (arrowheads) around CJ-2 particles (arrows) (B). Bar = 20 μm. Degeneration of alveolar walls (arrows) with increase in the number of activated macrophages (arrowheads) in lung from the mice instilled with CJ-2 particles and 50-nm gold nanoparticles (C). Bar = 50 μm.

Table 1. Lung lesion scoring and criteria*

Score	Histopathological lesion
0	No inflammatory changes
1	Alveolar edema and/or hemorrhage (±), mild bronchiolitis, and alveolitis
2	Alveolar edema and/or hemorrhage (±), moderate localized bronchiolitis, and alveolitis (at high magnification)
3	Alveolar edema, and/or hemorrhage (±), moderate multiple foci of bronchiolitis, and alveolitis (at low magnification)
4	Alveolar edema, and/or hemorrhage (+), severe diffuse bronchiolitis and alveolitis

* Modified from Naota et al. (2010).

Table 2. Lung lesion score

Group	Average score
Control (n = 6)	0
50-nm gold nanoparticles (n = 8)	0.5
CJ-2 + 50-nm gold nanoparticles (n = 8)	2.5*

*Significantly different from control group, $P < 0.05$.

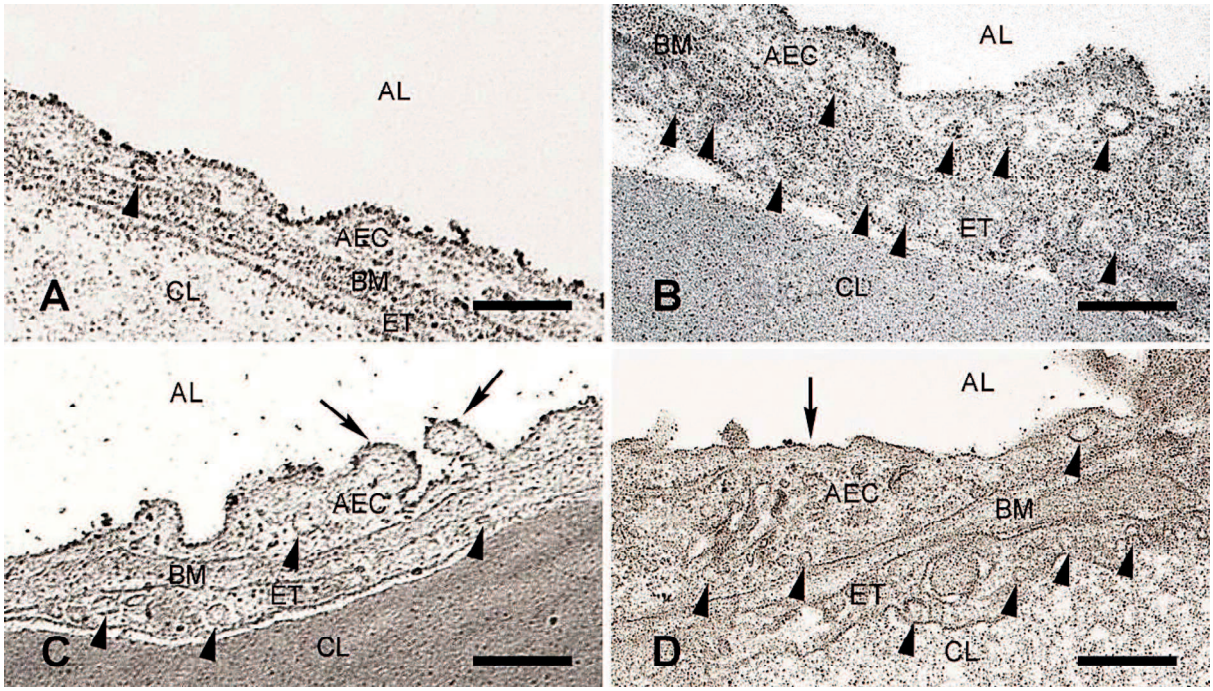

Figure 4. Transmission electron micrographs of lungs. The control lung shows thin alveolar wall with presence of endocytic vesicle (an arrowhead) in the cytoplasm of type I alveolar epithelial cell (A). Bar = 0.25 μm. Lung from the mice instilled with 50-nm gold nanopartilces alone shows increase in the number of endocytic vesicles (arrowheads) in the cytoplasm of type I alveolar epithelial cell and endothelial cell (arrowheads) (B). Bar = 0.5 μm. A ruffling of the surface of type I epithelial cell (arrows) and increase in the number of endocytic vesicles in the cytoplasm of type I epithelial cell and endothelial cell (arrowheads) in lung from the mice instilled with gold nanopartilces alone (C). Bar = 0.25 μm. Lung from the mice instilled with CJ-2 particles and gold nanoparticles shows swelling of type I alveolar epithelial cell (an arrow) with increase in the number of endocytic vesicles in the cytoplasm of type I epithelial cell and endothelial cell (arrowheads) (D). Bar = 0.5 μm. AL = alveolar lumen, AEC = alveolar epithelial cell, BM = basement membrane, ET = endothelial cell, CL = capillary lumen.

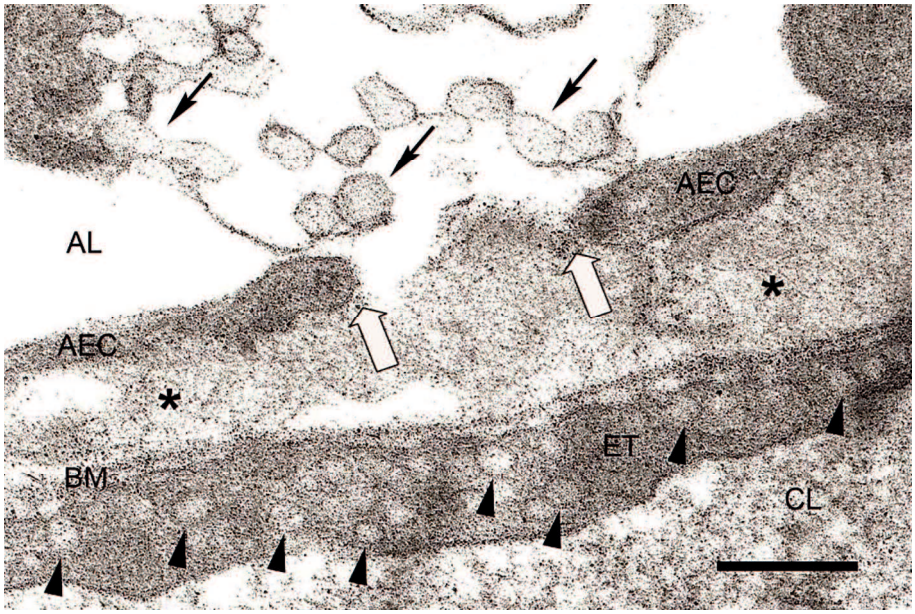

Figure 5. Transmission electron microscopic image of lung from the mice instilled with CJ-2 particles and 50-nm gold nanoparticles. Type I alveolar epithelial cell shows degenerative change (black arrows) with detachment of degenerated type I epithelial cell (white solid arrows) associated with interstitial edema (asterisks). Endothelial cells show increase in the number of endocytic vesicles in the cytoplasm (arrowheads). Bar = 0.5 μm. AL = alveolar lumen, AEC = alveolar epithelial cell, ET = endothelial cell, BM = basement membrane, CL = capillary lumen.

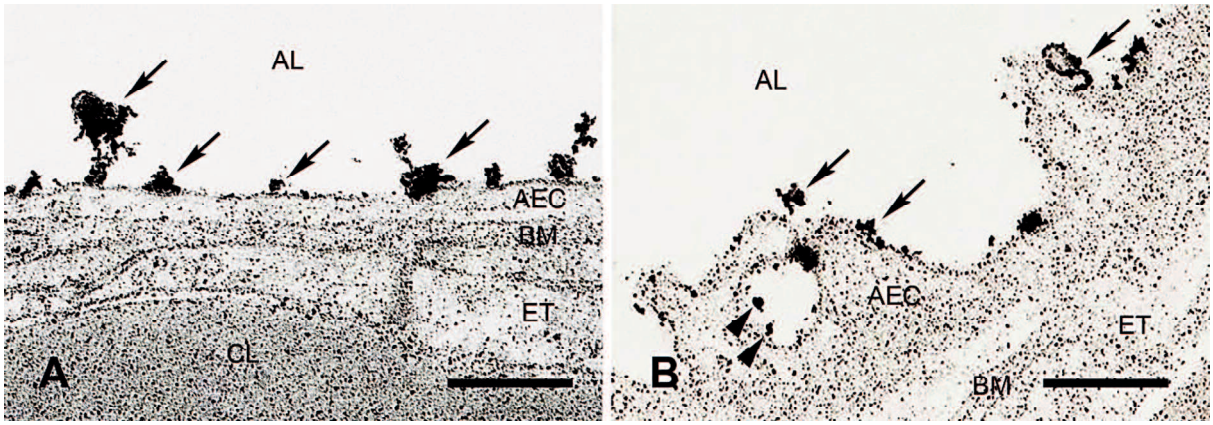

Figure 6. Transmission electron microscopic image of lung from the mice instilled with 50-nm gold nanoparticles alone. Attachment of gold nanoparticles to the surface of type I epithelial cell (arrows) (A). Bar = 0.5 μm. Presence of gold nanoparticles inside the endocytic vesicles in the cytoplasm of type I epithelial cell (arrowheads) and attachment of gold nanoparticles to the surface of type I epithelial cell (arrows) (B). Bar = 0.25 μm. AL = alveolar lumen, AEC = alveolar epithelial cell, BM= basement membrane, ET = endothelial cell, CL = capillary lumen

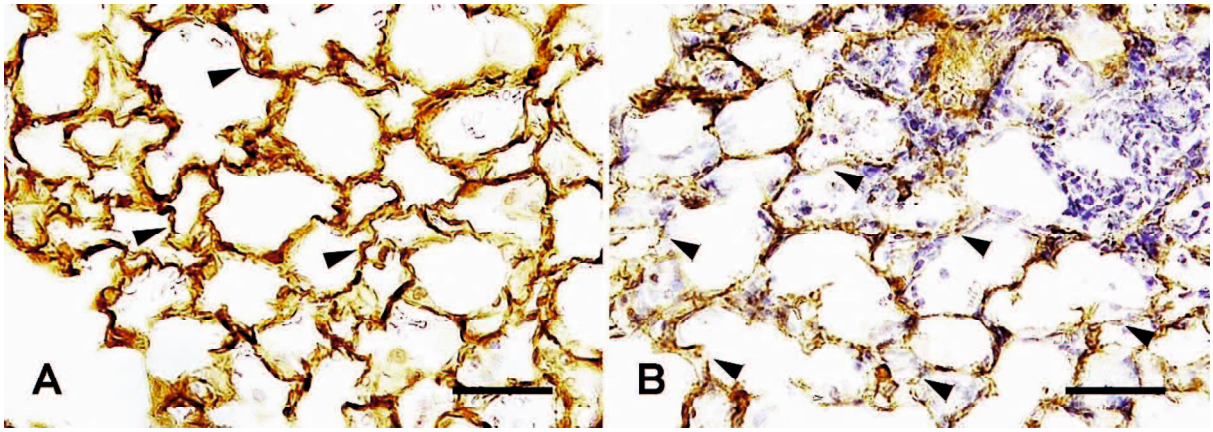

Figure 7. Laminin immunohistochemistry shows intense continuous positivity in the basement membrane of the alveolar wall (arrowheads) of lung from the mice instilled with 50-nm gold nanoparticles alone (A) and weaker discontinuous positivity (arrowheads) in lung from the mice instilled with CJ-2 particles and gold nanoparticles (B). Counterstained with hematoxylin. Bars = 50 μm.

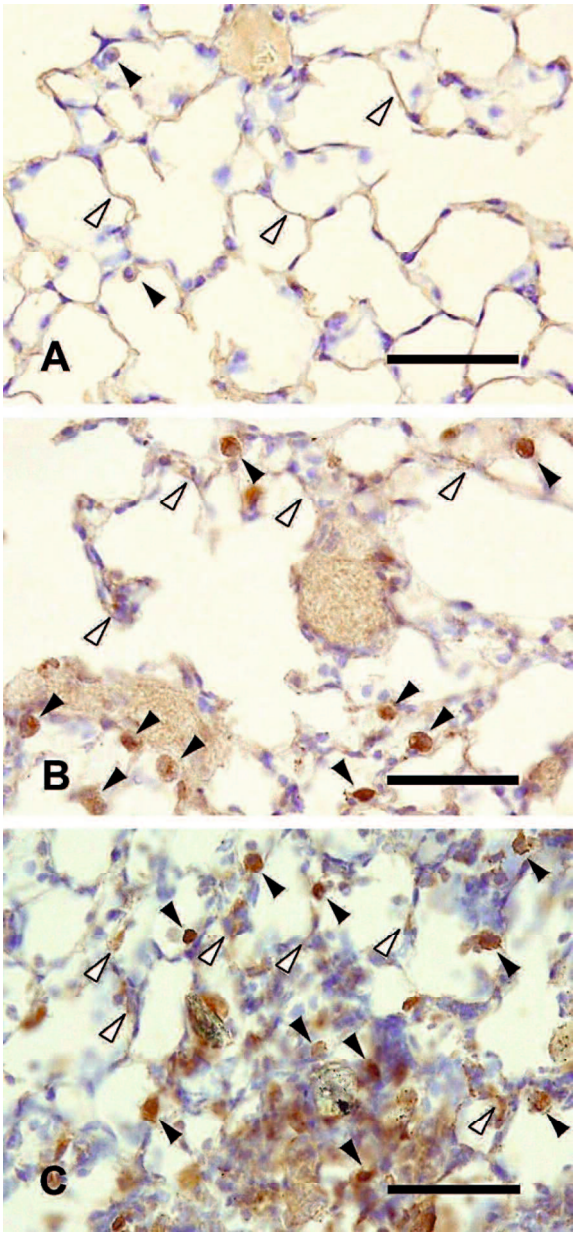

Figure 8. IL-6 immunohistochemistry shows mild positivity in alveolar macrophages (black arrowheads) with a weak expression in type I alveolar epithelial cells (white arrowheads) in lung from the control mice (A). Lung from the mice instilled with 50-nm gold nanoparticles alone shows more intense positivity in alveolar macrophages (black arrowheads) and type I alveolar epithelial cells (white arrowheads) (B). Lungs from the mice instilled with CJ-2 particles and gold nanoparticles show the most intense positivity in alveolar macrophages (black arrowheads) and type I alveolar epithelial cells (white arrowheads) (C). Counterstained with hematoxylin. Bars = 50 μm.

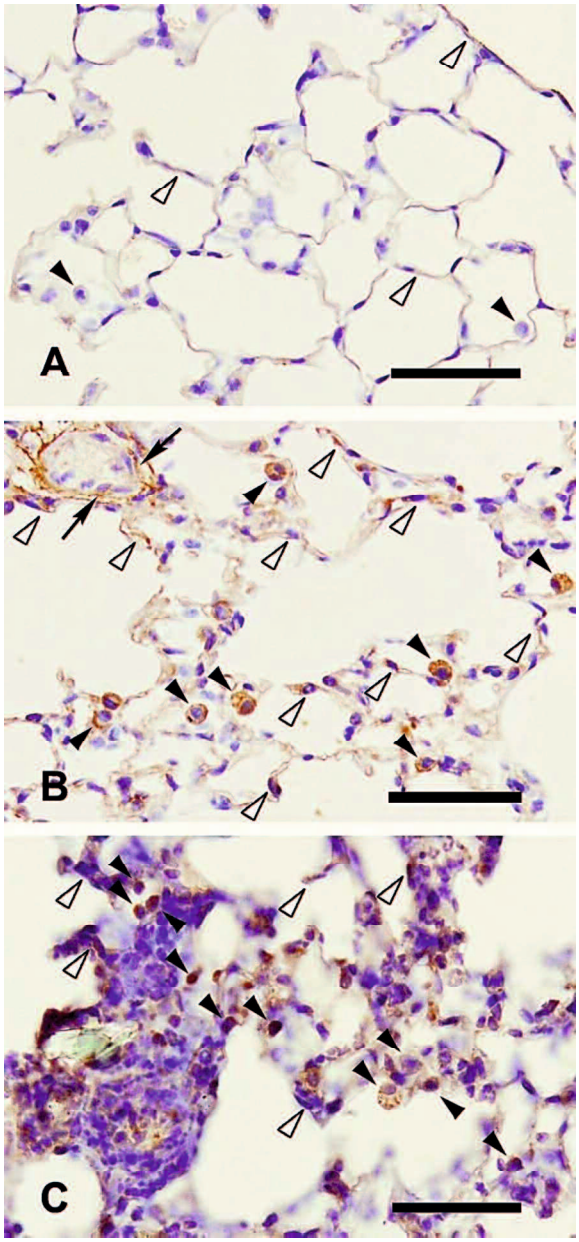

Figure 9. TNF-α immunohistochemistry shows mild positivity in alveolar macrophages (black arrowhead) with a weak expression in type I alveolar epithelial cells (white arrowheads) in lung from the control mice (A). Lung from the mice instilled with 50-nm gold nanoparticles alone shows more intense positivity in alveolar macrophages (black arrowheads), type I alveolar epithelial cells (white arrowheads) and endothelial cells (arrows) (B). Lungs from the mice instilled with CJ-2 particles and gold nanoparticles show the most intense positivity in alveolar macrophages (black arrowheads) and type I alveolar epithelial cells (white arrowheads) (C). Counterstained with hematoxylin. Bars = 50 μm.

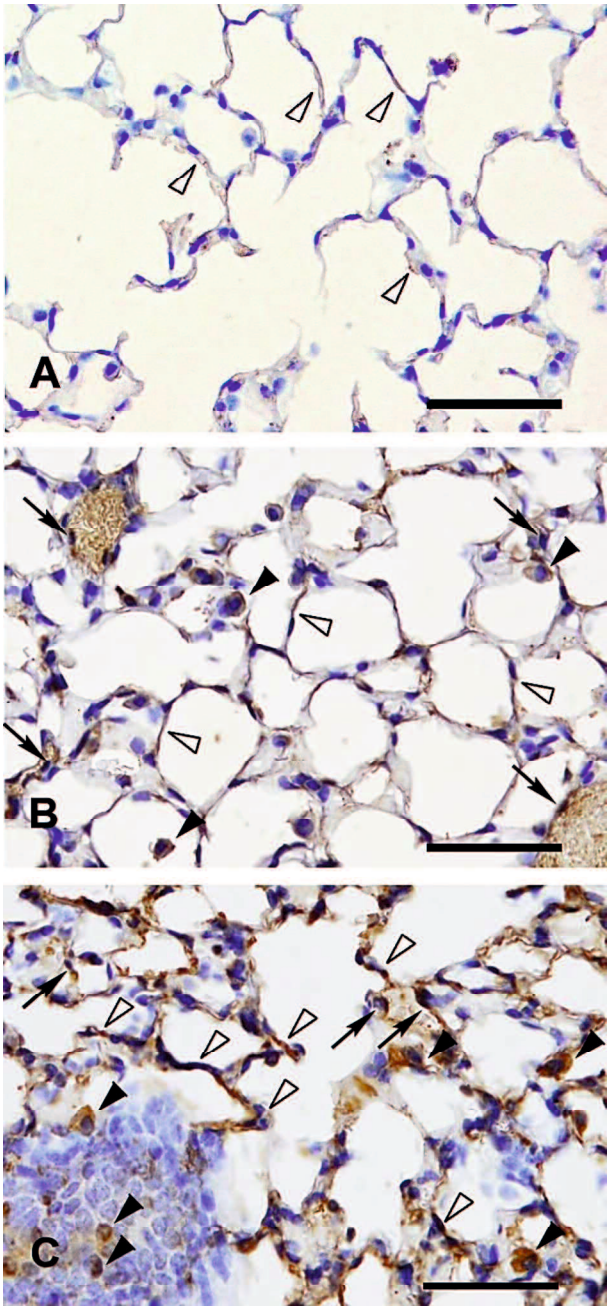

Figure 10. Cu/Zn SOD immunohistochemistry shows mild positivity in lungs from the control mice (A) and the mice instilled with 50-nm gold nanoparticles alone (B). Lungs from the mice instilled with CJ-2 particles and gold nanoparticles show more intense positivity (C). Cu/Zn SOD immunopositivity is observed in alveolar macrophages (black arrowheads) and type I epithelial cells (white arrowheads) and endothelial cells (arrows) (A, B and C). Counterstained with hematoxylin. Bars = 50 μm.

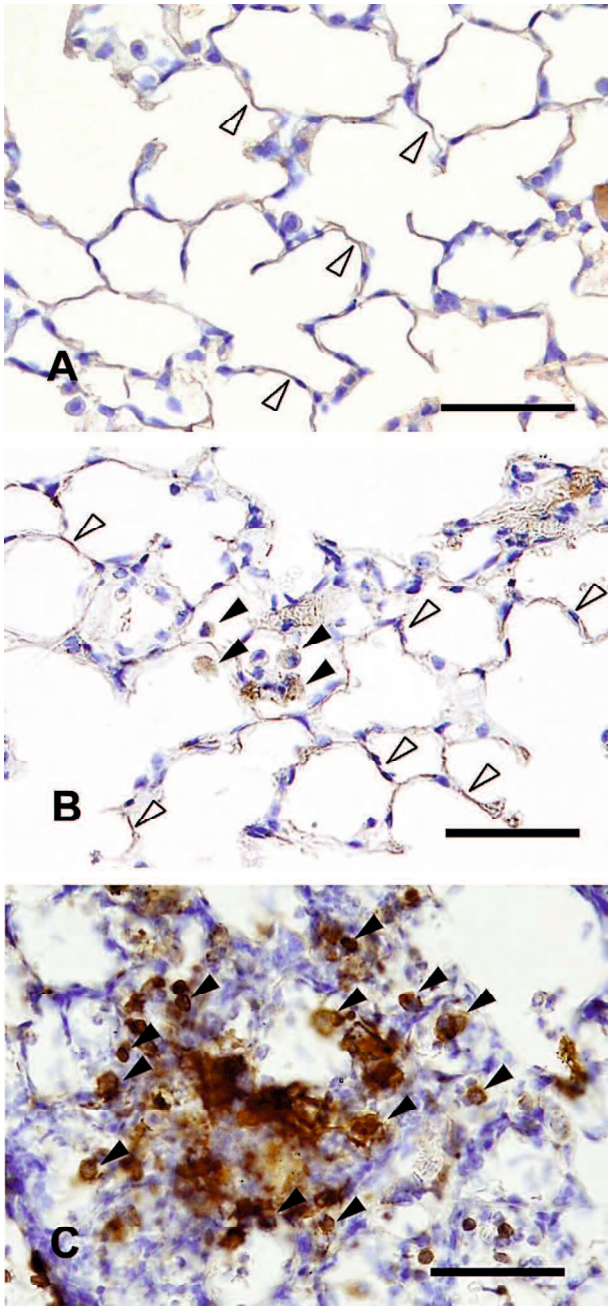

Figure 11. Inducible NOS (iNOS) immunohistochemistry shows mild positivity in type I alveolar epithelial cells (white arrowheads) and occasional weak positivity in macrophages (black arrowheads) in lung of the control mice (A) and the mice instilled with 50-nm gold nanoparticles alone (B). Intense iNOS immunopositivity is shown in alveolar macrophages (black arrowheads) in the inflammatory lesion in lung from the mice instilled with CJ-2 particles and gold nanoparticles (C). Counterstained with hematoxylin. Bars = 50 μm.

Table 3. Number of inflammatory cells with positive immunolabeling[†]

Group	TNF-α	IL-6
Control (n = 6)	45.0 ± 7.39	33.8 ± 5.27
50-nm gold nanoparticles (n = 8)	108.1 ± 12.32[*]	74.9 ± 4.16[*]
CJ-2 + 50-nm gold nanoparticles (n = 8)	154.0 ± 8.10[*,a]	126.5 ± 11.13[*,a]

[†]Number of cell per 94,850 μm^2 of 4-μm-thick paraffin section, mean ± standard error
[*]Significantly different from control group, $P < 0.05$.
[a]Significantly different from 50-nm gold nanoparticles instillation alone group, $P < 0.05$.

Table 4. Bronchoalveolar lavage fluid analytical parameters

Group	Neutrophils ($\times 10^3$)	Macrophage ($\times 10^3$)	Cell viability (%)
Control (n = 3)	5.6 ± 4.8	57.4 ± 25.0	84.1 ± 2.4
50-nm gold nanoparticles (n = 4)	3.3 ± 0.7	118.9 ± 30.0[*]	89.7 ± 0.7
CJ-2 + 50-nm gold nanoparticles (n = 4)	255.5 ± 4.4[*,a]	161.3 ± 14.5[*,a]	89.7 ± 3.2

Values are the mean ± standard error.

[*]Significantly different from control group, $P < 0.05$.

[a]Significantly different from 50-nm gold nanoparticles instillation alone group, $P < 0.05$.

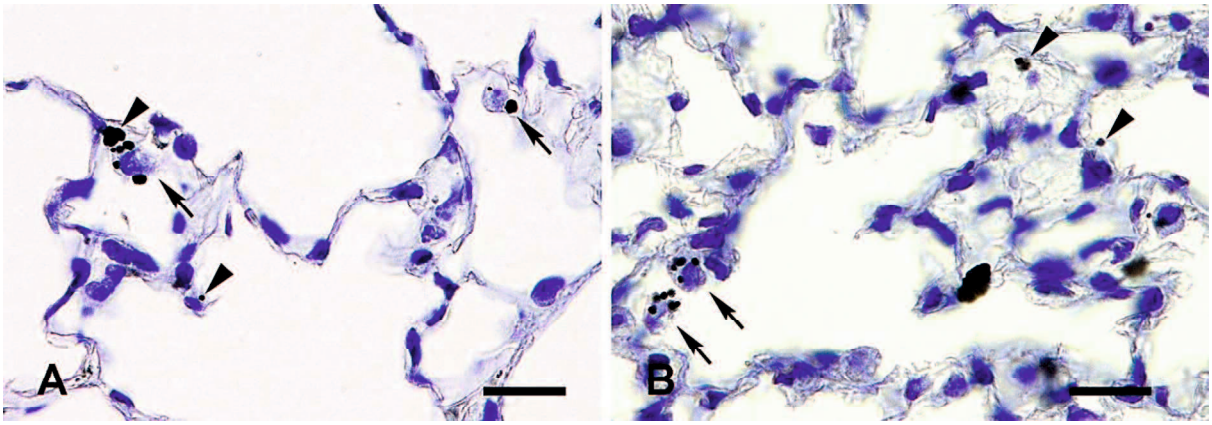

Figure 12. Silver-enhanced autometallography shows presence of gold nanoparticles in alveolar macrophages (arrows) and the surface of the alveolar lumen (black arrowheads) in lung from the mice instilled with 50-nm gold nanoparticles alone (A) and lung instilled with CJ-2 particles and gold nanoparticles (B). Counterstained with hematoxylin. Bars = 10 μm.

CHAPTER 2

Demonstration of the Clathrin- and Caveolin-Mediated Endocytosis at the Maternal–Fetal Barrier in Mouse Placenta after Intravenous Administration of Gold Nanoparticles

ABSTRACT

Exposure to nanoparticles during pregnancy is a public concern, because it has been reported that nanoparticles may pass from the mother to the fetus across the placenta, resulting in death of fetus. The purpose of this study was to determine the possible translocation pathway of gold nanoparticles across the maternal–fetal barrier as well as the toxicity of intravenously administered gold nanoparticles to the placenta and fetus. Pregnant ICR mice were intravenously injected with 0.01% of 20- and 50-nm gold nanoparticle solutions on the 16^{th} and 17^{th} days of gestation. There was no sign of toxic damage to the placentas, and maternal and fetal organs of the mice treated with 20- and 50-nm gold nanoparticles. ICP-MS analysis demonstrated significant amounts of gold deposition in the maternal livers and placentas, but no detectable level of gold in the fetal organs. However, electron microscopy demonstrated an increase of endocytic vesicles in the cytoplasm of syncytiotrophoblasts and fetal capillary endothelial cells in the maternal–fetal barrier of mice treated with gold nanoparticles. Clathrin immunohistochemistry and immunoblotting showed increased immunoreactivity of clathrin protein in the placental tissues of mice treated with 20- and 50-nm gold nanoparticles. Clathrin immunopositivity was observed in syncytiotrophoblasts and fetal endothelial cells. In contrast, caveolin-1 immunopositivity was observed exclusively in the fetal endothelium. These findings suggested that intravenous administration of gold nanoparticles might upregulate clathrin- and caveolin-mediated endocytosis at the maternal–fetal barrier in mouse placenta.

INTRODUCTION

The development of nanotechnology has resulted in rapid expansion of the use of nanoparticles in various categories, e.g., food, cosmetic, electronic, medical and pharmaceutical industries (Kulvietis et al. 2011; Saduaskas et al. 2009b; Saunders 2009; Sung et al. 2001; Yamashita et al. 2011; Yang et al. 2008). Because nanoparticles have properties, such as an extremely small size (less than 100 nm in diameter), high surface area per mass ratio, and high potential chemical activities, an adverse health effects from the daily application of nanoparticles have been seriously considered (Cartwright et al. 2012; Elsaesser and Howard 2012; Ema et al. 2010; Myllynen et al. 2008; Saunders 2009; Shukla et al. 2005). The fetus is known to be susceptible to various toxic substances (Austin et al. 2011; Kulvietis et al. 2011; Yamashita et al. 2011). Therefore, there is high concern regarding exposure to exogenous substances, including nanosized materials for pregnant women (Keelan 2011; Saunders 2009; Yamashita et al. 2011).

The placenta is the organ that connects the maternal and fetal circulation. Oxygen and nutrient exchanges between the mother and fetus occur in the maternal–fetal barrier at the labyrinthine zone of the placenta (Buerki-Thurnherr et al. 2012; Furukawa et al. 2011; Khan et al. 2011; Kirby and Bradbury 1965; Takata et al. 1997). In addition, toxic substances can be also transferred across the maternal–fetal barrier. Therefore, the placenta is a critical site for fetal intoxication (Ema et al. 1010; Keelan 2011; Saunders 2009). Placental structure differs among animals. Humans and rodents have the same type of placenta, hemochorial type. There are, however, there are some differences in the placental structures between humans and rodents (Keelan 2011; Yamashita et al. 2011). Human maternal–fetal barrier consists of one trophoblastic layer (syncytiotrophoblast layer) on the maternal side with underlying discontinuous cytotrophoblastic layer, basement membrane and fetal endothelial

cells on the fetal side. In contrast, mouse maternal–fetal barrier has three trophoblastic layers on the maternal side that connect each layer with tight gap junction with underlying fetal endothelial cells on the fetal side (Khan et al. 2011; Kirby and Bradbury 1965; Kulvietis et al. 2011; Saunders 2009). Despite such anatomical differences, rodent placentas are regarded as advantage of the ethical reason and similarities in placental functions like humans, and have been used in every stage of pregnancy (Keelan 2011; Mohanty et al. 2010; Yamashita et al. 2011).

The mechanisms of placental exchange for several endogenous substances include passive and facilitated diffusion, via transtrophoblastic channels, and active transport (e.g. via endocytosis) (Buerki-Thurnherr et al. 2012; Kulvietis et al. 2011; Saunders 2009). Endocytosis may be an important mechanism for certain types of nanoparticle translocation across the maternal–fetal barrier (Buerki-Thurnherr et al. 2012; Kulvietis et al. 2011; Saunders 2009). Macropinocytosis and classical clathrin-dependent, non-classical clathrin-independent (caveolae-dependent) or clathrin- and caveolae-independent endocytosis are further proposed as subtypes of endocytosis (Conner and Schmid 2003; Le Roy and Wrana 2005; McMahon and Boucrot 2011; Myllynen et al. 2008). Clathrin, a major protein of clathrin-coated endocytic vesicles, and caveolin-1, a major protein of the caveolae structure (Mohanty et al. 2010), are expressed in trophoblasts and endothelial cells of the human placenta in physiological condition. However, information about the expression of clathrin and caveolin-1 in the placental tissue during nanoparticle exposure remains unclear. Therefore, the present study aimed to examine the clathrin- and caveolin-mediated endocytosis after intravenous administration of gold nanoparticles in mouse placenta.

MATERIALS AND METHODS

Animals

Sixteen pregnant ICR mice at gestation day 16 (GD16) (15–17 weeks old, 55–75 g) were obtained from CLEA Japan Inc. (Tokyo, Japan). Commercial diet CE-2 (CLEA Japan Inc.) and tap water were given *ad libitum* throughout the experiment. The mice were housed at approximately 25°C and 55–70% relative humidity under a 12-hr light/dark cycle. The experiments were approved by the Institutional Animal Care and Use Committee, and all procedures were conducted according to the Tottori University guidlines for animal welfare.

Particles

Morphology of gold nanoparticles

The experiment employed 20- and 50-nm colloidal gold solutions (mean diameters of 19.6 nm and 49.3 nm respectively, according to the manufacturer's information; BB International, Cardiff, UK). The morphology of the gold nanoparticles was examined by transmission electron microscopy (TEM-100CX; Japan Electron Optical Laboratory, Tokyo, Japan). The 20-nm and 50-nm colloidal gold solutions contained electron-dense, spherical, uniform, and individual or slightly agglomerated particles (Figure 1).

Experimental protocol

At GD16, pregnant ICR mice were intravenously injected with 0.5 ml of saline solution (control, $n = 4$), 20-nm, or 50-nm colloidal gold solutions through the tail vein ($n = 6$

per treatment). At 24 hr after the first injection, the pregnant mice (GD17) were intravenously injected with the same solutions as the previous injections. At 24 hr after the second injection, the pregnant mice (GD18) were sacrificed by performing exsanguination under deep anesthesia induced by the intraperitoneal injection of sodium pentobarbital. Then, tissue samples were collected (Figure 2).

Sampling for maternal organs, plancentas and fetal organs

Maternal livers, placentas, and fetal livers were collected from the pregnant mice and fetuses after gross examination. The samples were used for histopathological, immunohistochemical, autometallography (AMG) and transmission electron microscopic examinations.

Inductively coupled plasma-mass spectroscopy (ICP-MS)

Maternal livers, placentas, and fetal livers (0.1 g of each tissue; $n = 2$ from the control or $n = 3$ from mice that were injected with gold nanoparticles) were digested with 2 ml of aqua regia. After digestion the inorganic residues were dissolved in 5 ml of 0.05 N HCl and ultrasonicated for 20 min, and the samples were then analyzed by performing inductively coupled plasma-mass spectroscopy (ICP-MS) (HP 4500; Agilent Technologies, Santa Clara, CA, U.S.A.). Detection and quantification limits for gold were 0.5 ng/ml and 1 ng/ml, respectively (Sonavane et al. 2008).

Histopathology

Maternal livers, placentas and fetal livers were fixed in 10% neutral-buffered formalin. The formalin-fixed tissues were processed using routine pathological methods and embedded in paraffin blocks. Paraffin-embedded thin sections (4-μm-thick) were applied for hematoxylin and eosin staining, immunohistochemistry and AMG. Histopathological examination was performed by 2 pathologists in a blind manner under a light microscope.

Autometallography (AMG)

Paraffin-embedded thin sections of placenta, maternal liver, and fetal liver were used for AMG staining (Danscher 1984; Danscher and Stoltenberg 2006). The sections were treated with a physical developer consisting of 50% gum arabic, 50% citrate buffer, 5.6% hydroquinone, and 17% silver nitrate. The reaction was conducted in a water bath at 26°C for 1 hr in the dark. Excessive silver residue was removed with a 5% sodium thiosulfate solution for 10 min. Next, the sections were counterstained with hematoxylin. A positive result was demonstrated as small black silver grains inside the cells of interest.

Immunohistochemistry

Paraffin-embedded sections of the placentas were used for the immunohistochemical detection of clathrin, caveolin, interleukin (IL)-6, tumor necrosis factor (TNF)-α, dimeric copper- and zinc-containing superoxide dismutase (Cu/Zn SOD), inducible nitric oxide synthase (iNOS) and caspase-3. For antigen retrieval, the sections were treated with citrate buffer (pH 5.4) and then microwaved. Endogenous peroxidase activity was quenched with 3% H_2O_2 at room temperature for 30 min. The slides were then blocked with 10% normal goat serum or 10% bovine serum albumin (for the detection of IL-6) for 5 min in a

microwave. Next, the sections were incubated with primary antibodies at 4°C overnight (anti-clathrin heavy chain: Abcam, Cambridge, MA, U.S.A. 1:7,000 dilution; anti-caveolin-1: Santa Cruz Biotechnology, Santa Cruz, CA, U.S.A. 1:1,500 dilution; anti-IL-6: Santa Cruz Biotechnology 1:200 dilution; TNF-α: Monosan, Uden, the Netherlands, 1:15 dilution; anti-Cu/Zn SOD: Stressgen Bioreagents, Victoria, Canada, 1:200 dilution; anti-iNOS: BD Transduction Laboratories, Lexington, KY, U.S.A. 1:125 dilution; and anti-caspase-3: Promega, Madison, WI, U.S.A 1:250) or an equivalent amount of phosphate-buffered saline as a negative control. A labeled streptavidin biotin kit (Dako, Glostrup, Denmark) was used to detect immunoreaction complexes in the avidin–biotin complex assay. Positive immunoreactions appeared as brown staining with 3,3′-diaminobenzidine tetrahydrochloride (DAB). The sections were counterstained with hematoxylin and observed by light microscopy in 4 randomly selected lesions at ×100 magnification. Positive immunolabeling areas were analyzed in 5 randomly selected areas from each mouse by Image-Pro Plus 6.1 software (MediaCybernetics, Inc., Silver Spring, MD, U.S.A.).

Double immunofluorescence

The sections were placed in citrated buffer solution (pH = 5.4), microwaved and then treated with proteinase K for 15 min for antigen retrieval. Next, the sections were incubated with normal goat serum for 5 min in a microwave. After incubation with normal goat serum, the sections were applied to the primary antibodies against clathrin (1:500 dilution) or caveolin-1 (1:350 dilution) overnight at 4°C and then incubated with Alexa Fluor 488-conjugated secondary antibody (1:200 dilution) for 1 hr at room temperature. Then, the sections were reacted with primary antibody against cytokeratin (Dako, 1:100 dilution) overnight at 4°C and then incubated with Alexa Fluor 555-conjugated secondary antibody

(1:300 dilution) for 30 min at room temperature. Thereafter, the sections were mounted in plain 80% Tris-buffered glycerol. Analyses were performed with a confocal imaging system (AX-70, Olympus Laboratory, Tokyo, Japan).

Electron microscopy

Half of the longitudinal sections from the placenta were cut into cubes measuring 1–2 mm^3. Next, tissues were fixed in glutaraldehyde for 3 hr at 4°C, rinsed in 0.1 M phosphate buffer (pH 7.4), postfixed with 1% osmium tetroxide for 1 hr, dehydrated in alcohol and embedded in epoxy resin. The areas of interest were selected for electron microscopy examination from 1% toluidine-stained semi-thin (1-μm-thick) sections and subsequently cut into ultra-thin (70-nm-thick) sections. After staining with uranyl acetate and lead citrate, ultra-thin sections were examined using a transmission electron microscope (TEM-100CX; Japan Electron Optical Laboratory, Tokyo, Japan).

Western blot analysis

Approximately 100 mg of placental tissue (n = 4 per mouse) was harvested and processed in lysis buffer (Roche, Basel, Switzerland) to extract protein. Tissue lysates were clarified by centrifugation at 14,000 rpm for 10 min, and the protein content of the supernatant was determined. Lysate supernatants were diluted 1:1 with 2× electrophoresis sample buffer (1× sample buffer = 125 mM Tris–HCl, pH 6.8, 2% sodium dodecyl sulfate [SDS], 5% glycerol, 0.003% bromophenol blue and 1% β-mercaptoethanol) and aliquots equivalent to 20 μg of total protein per sample were resolved in a 15% SDS/polyacrylamide gel. The gels were electroblotted onto a polyvinylidene difluoride membrane (BioRad,

Hertfordshire, U.K.), and the membrane was probed with the primary antibodies, rabbit anti-clathrin heavy chain (1:1,000 dilution) or rabbit anti-caveolin-1 (1:1,000 dilution). After overnight incubation at 4°C, the membrane was washed and probed with the secondary antibody, which was an anti-rabbit horse radish-peroxidase-conjugated IgG. After incubation for 1 hr, the membrane was washed by washing buffer. The immunoblot procedure was performed using the chemiluminescence detection reagent (Luminata™ Forte Western HRP Substrate, Millipore, Billerica, MA, U.S.A.) according to the manufacturer's protocol. The bands on the clarified blots were measured with an image analysis system (Image-Pro Plus 6.1, MediaCybernetics, Inc., Silver Spring, MD, U.S.A.), and the digital numbers obtained were integrated density values of the intensity of each band.

In situ apoptosis detection (TUNEL assay)

Paraffin-embedded thin sections of placenta were treated with proteinase K at room temperature. Then, the sections were inactivated for endogenous peroxidase by applying 3% H_2O_2 for 5 min. After washing, the labeling reaction mixture (consisting of TdT enzyme and labeling safe buffer, *in situ* apoptosis detection kit: Takara Bio Inc., Otsu, Japan) was applied to the sections, and they were incubated in a 37°C humidified chamber for 70 min. Then, the sections were treated with Anti-FITC HRP conjugate (Takara Bio Inc.) and incubated at 37°C for 30 min. After coloring with DAB, the sections were counterstained with 3% methyl green and observed under a light microscope.

Statistical analysis

All of the data were expressed as the mean ± standard error (S.E.). Statistical significance was determined by performing the Mann-Whitney's U-test or the Student's *t*-test

for 2-group comparisons. For all comparisons, P values less than 5% ($P < 0.05$) were considered statistically significant.

RESULTS

ICP–MS

Gold was detected in the maternal livers and placentas from mice injected with 20- and 50-nm gold nanoparticles (Table 1). The level of gold in both maternal livers and placentas from the mice injected with 20-nm gold nanoparticles was significantly higher than the level of gold from the mice injected with 50-nm gold nanoparticles. Gold was not detected in maternal livers and placentas from the control mice and fetal livers from the control mice and the mice injected with 20- and 50-nm gold nanoparticles.

Histopathology

Placental tissues from the mice injected with 20- and 50-nm gold nanoparticles did not show any significant pathological changes at the maternal–fetal barrier in the labyrinthine zone of the placentas compared to the control mice (Figure 3). Only mild swelling of the cytoplasm of syncytiotrophoblastic cells and fetal endothelial cells in the maternal–fetal barrier from the mice injected with gold nanoparticles were occasionally observed (Figures 3B and 3C).

No pathological lesions were found in other maternal and fetal organs from the control mice and the mice injected with 20- and 50-nm gold nanoparticles.

Autometallography

Silver-enhanced gold nanoparticles were detected in Kupffer cells in the maternal livers of mice injected with 20- and 50-nm gold nanoparticles (Figures 4B and 4C). Gold nanoparticles were not detected by the AMG method in the placentas, maternal livers, and fetal livers from the control mice and placentas and fetal livers from the mice injected with 20- and 50-nm gold nanoparticles (Figure 4).

Immunohistochemistry

Clathrin immunohistochemistry demonstrated positive reaction in syncytiotrophoblastic cells and fetal endothelial cells (Figure 5). Weak positivity was observed in syncytiotrophoblastic cells and fetal endothelial cells at the maternal–fetal barrier from the control mice (Figure 5A) compared to the mice injected with gold nanoparticles (Figures 5B and 5C). The image analysis of clathrin immunopositivity showed higher intensity in the placental tissues from the mice injected with gold nanoparticles. No significant differences were observed between clathrin immunoreactivity in the placental tissues from the mice injected with 20- and 50-nm gold nanoparticles and that seen by image analysis (Table 2).

Caveolin-1 immunoreactivity was detected exclusively in the cytoplasm of fetal endothelial cells at the site of maternal–fetal barrier in the labyrinthine zone of the placentas (Figure 6). The positivity of caveolin-1 immunolabeling was lesser in the placental tissues from the control mice (Figure 6A) compared to the mice injected with gold nanoparticles (Figures 6B and 6C). The image analysis of caveolin-1 immunolabeling showed higher intensity in the placental tissues from the mice injected with gold nanoparticles. No significant differences were observed between caveolin-1 immunoreactivity in the placental

tissues from the mice injected with 20- and 50-nm gold nanoparticles and that seen by image analysis (Table 2).

There were occasional positive findings in IL-6, TNF-α, Cu/Zn SOD and iNOS immunolabeling in the cytoplasm of syncytiotrophoblasts and fetal endothelial cells in the maternal–fetal barrier. No difference in the intensity and distribution of IL-6, TNF-α, Cu/Zn SOD and iNOS immunolabeling between the control mice and the mice injected with 20- and 50-nm gold nanoparticles was observed. No positivity in caspase-3 immunolabeling was detected in the maternal–fetal barrier from the control mice and the mice injected with 20- and 50-nm gold nanoparticles.

Double immunofluorescence

Positive clathrin immunoreactivity was demonstrated in the syncytiotrophoblast layer and fetal vascular endothelium (Figure 7A). The co-localization of clathrin and cytokeratin was observed in the syncytiotrophoblast layer (Figure 7C). In contrast, caveolin-1 immunoreactivity revealed strong immunoreactivity exclusively in fetal capillary endothelial cells (Figure 8A). The co-localization of caveolin-1 and cytokeratin was not observed in the labyrinthine zone of the placentas (Figure 8C).

Electron microscopy

The maternal–fetal barrier in the labyrinthine zone of the placentas from the control mice consisted of 3 layers of syncytiotrophoblastic cells (syncytiotrophoblast layers I, II, and III) with underlying fetal capillary endothelial cells. Electron microscopy demonstrated no signs of cell/tissue damage in the placenta from the mice treated with gold nanoparticles.

Numerous microplicae and infolding with a few vesicle-like structures were observed in the cytoplasm of syncytiotrophoblast layers II and III in the maternal–fetal barrier from the control mice (Figure 9A). Moderate enlargement with an increase in the number of vesicle-like structures were observed in the cytoplasm of syncytiotrophoblast layers II and III in the maternal–fetal barrier from the mice injected with 20- and 50-nm gold nanoparticles (Figures 9B, 9C and Figure 10). An increase in the number of vesicle-like structures was also shown in the capillary endothelial cells in the maternal–fetal barrier from the mice injected with 20- and 50-nm gold nanoparticles compared to the control mice (Figure 9C and Figure 10).

Western blot analysis

Immunoblotting of tissue lysates from placentas of the mice injected with 20- and 50-nm gold nanoparticle solutions demonstrated a 171-kDa band of clathrin protein. The positive band from the control mice was less intense compared to positive bands from the mice injected with gold nanoparticles (Figure 11A). The integrated density values of the intensity of bands of tissue lysates from the mice injected with gold nanoparticles were significantly greater than that of the control mice (Table 3).

A 22-kDa band representing caveolin-1 was observed in the placental tissue lysates. The positive bands showed no difference in intensity in the placental lysates from the control mice and the mice injected with gold nanoparticles (Figure 11B). The integrated density values of the intensity of bands of the tissue lysates were not significantly different among all groups (Table 3).

In situ apoptosis detection (TUNEL assay)

The TUNEL assay showed negative results in the labyrinthine zone of the placentas of the control, 20- and 50-nm gold nanoparticle injected mice (data not shown).

DISCUSSION

At present, the risk of exposure to nanosized materials in pregnancy is increasing. On the other hand, there are only a few studies on the translocation pathway of nanoparticles across the maternal–fetal barrier (placental barrier) (Cartwright et al. 2012; Elsaesser and Howard 2012; Kulvietis et al. 2011). The present study aims to determine the possible translocation mechanism of gold nanoparticles across the maternal–fetal barrier of mice.

ICP-MS analysis demonstrated a significant amount of gold deposited in the maternal livers and placentas but no detectable level of gold in the fetal organs. Although AMG staining also showed the dominant accumulation of gold nanoparticles in Kupffer cells in the livers of the pregnant mice, no AMG positive findings were observed in the fetuses after intravenous administration. The liver is a major organ for the elimination of circulating nanoparticles (Sadauskas et al. 2009a). A previous study also reported that gold nanoparticles are primarily phagocytized by Kupffer cells and that almost of the administered nanoparticles present in the liver after intravenous administration in rodents (Balasubramaniun et al. 2010; Sadauskas et al. 2007; Sadauskas et al. 2009a; Semmler-Behnke et al. 2008).

No pathological changes were observed in the placentas, maternal organs, and fetal organs from mice treated with 20-nm and 50-nm gold nanoparticle solutions, suggesting that gold nanoparticles would not be harmful to pregnant mice and their placentas at the doses that we used. Previous *in vitro* and *in vivo* studies also reported that various sizes and doses of gold nanoparticles showed no obvious toxicity in mice and rats (Lasagna-Reeves et al. 2010; Sadauskas et al. 2009b; Semmler-Behnke et al. 2008).

Previous studies on the translocation pathway of nanoparticles across the fetal–maternal barrier of the human placenta suggest that endocytosis plays an important role in the transportation of nanoparticles (Keelan 2011; Kulvietis et al 2011; Saunders 2009; Wick et al.

2010). In the present study on the mouse placenta, an increase in the number of endocytic vesicles was also observed in the cytoplasm of the syncytiotrophoblasts and fetal endothelial cells by electron microscopy, suggesting that endocytosis might be upregulated in the maternal–fetal barrier after administration of gold nanoparticle solutions. Endocytosis plays an important role for the transport of nutrients or biomolecules, such as albumin, folic acid, hormones, etc. at the placenta in the physiological condition (Lambot et al. 2006; Pelkmans and Helenius 2002).

Clathrin-mediated endocytosis was previously described in the cytoplasm of syncytiotrophoblasts of the mouse placenta (Lambot et al. 2006). Clathrin-mediated endocytosis is involved in the recycling of albumin in the term placenta, neurotransmitter transport, and the internalization of several antigens (Lambot et al. 2006; McMahon and Boucrot 2011; Mousavi et al. 2004). In this study, clathrin immunohistochemistry showed an increase of intense positivity in the endocytic vesicles of both syncytiotrophoblasts and fetal endothelial cells. The localization of clathrin expression was confirmed by performing double immunofluorescence by using antibodies to clathrin and cytokeratin. Clathrin was also demonstrated in the syncytiotrophoblasts and fetal capillary endothelium. Immunoblot analysis showed an increase in clathrin protein expression in the placental tissues from mice treated with gold nanoparticles. These results suggested that gold nanoparticle administration upregulates clathrin expression in the placenta and that clathrin-mediated endocytosis might be one of the pathways of gold nanoparticle translocation in the maternal–fetal barrier.

Caveolae-mediated endocytosis is also considered to be one of the pathways for the translocation of nanoparticles in the air–blood barrier (Naota et al. 2013). Caveolin-1 protein plays a role in the regulation of caveolar invagination and the formation of caveolae, which is one form of the endocytic vesicle (Linton et al. 2003; Nabi and Le 2003; Pelkmans and Helenius 2002; Rothberg et al. 1992). In murine placental tissues, the localization of

caveolin-1 has been demonstrated in the vasculatures, especially in the fetal vascular endothelium (Bryne et al. 2007; Lyden et al. 2002; Mohanty et al. 2010). In this study, increased intensity of caveolin-1 immunohistochemistry was observed exclusively in the fetal endothelium after the administration of gold nanoparticle solutions. In contrast, immunoblotting showed no difference in the amount of caveolin-1 expression between the control mice and the mice treated with gold nanoparticles, suggesting the possible re-assembly of caveolin-1 protein from the cytosol to the caveolae structure.

In this study with the experimental design, applied techniques including electron microscopy failed to detect signs of actual translocation of the exposed particles as well as signs of their toxicity. However, an increase of endocytic vesicles in the cytoplasm of syncytiotrophoblasts and fetal endothelial cells in the maternal–fetal barrier of mice treated with gold nanoparticles was demonstrated. A further study with prolonged duration, different kinds of nanoparticles and sensitive techniques for the detection of nanoparticles are required to ascertain whether exposed nanoparticles may have a chance to be translocated through the maternal–fetal barrier by both clathrin-mediated and caveolae-mediated endocytosis demonstrated in this study.

FIGURES AND FIGURE LEGENDS

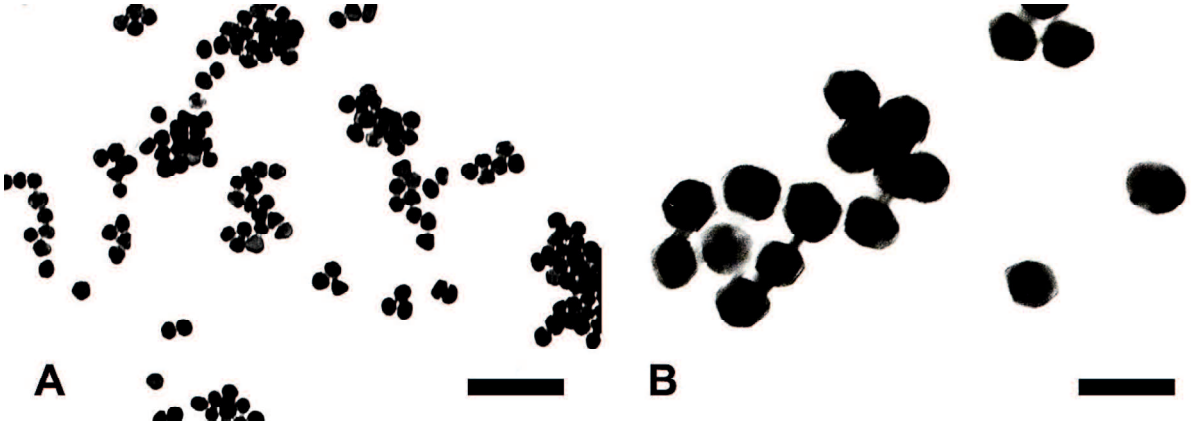

Figure 1. Electron micrographs of 20-nm (A) and 50-nm (B) gold nanoparticles show electron-dense, spherical, uniform, and individual or slightly agglomerated appearance. Bar = 100 nm.

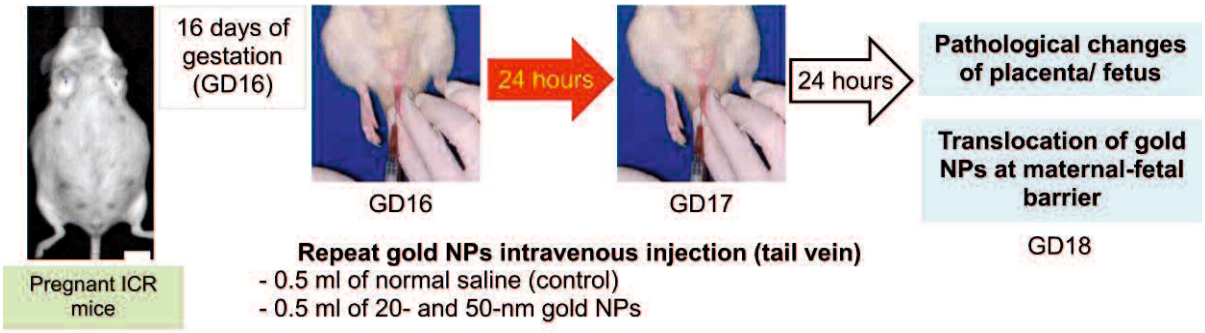

Figure 2. Schematic diagram shows the materials and methods of the experiment. At the 16th day of gestation (GD16), pregnant ICR mice were intravenously injected with 0.5 ml of saline solution, 20-nm, or 50-nm gold nanoparticles (NPs) through the tail vein. At 24 hr after the first injection, the pregnant mice (GD17) were intravenously injected with the same solutions as the previous injections. At 24 hr after the second injection, the pregnant mice (GD18) were sacrificed. Tissue samples were collected for the pathological examination and the investigation of the translocation pathway of gold nanoparticles at the maternal–fetal barrier.

Table 1. Gold contents in the tissues measured by ICP-MS.

Group		Gold content (μg/g dry tissue)		
		Maternal liver	Placenta	Fetal liver
Control	(n = 2)	0.2 ± 0.07	ND	ND
20-nm gold NPs	(n = 3)	640.3 ± 171.80[a]	1.3 ± 0.61	ND
50-nm gold NPs	(n = 3)	99.2 ± 2.75[b]	1.0 ± 0.78	ND

Values are the mean ± standard error.
[a]Significantly different between the control and 20 nm gold NPs injected mice, $P < 0.05$.
[b]Significantly different between 20-nm gold NPs injected mice and 50-nm gold NPs injected mice, $P < 0.05$.
NPs = nanoparticles
ND = Not detected.

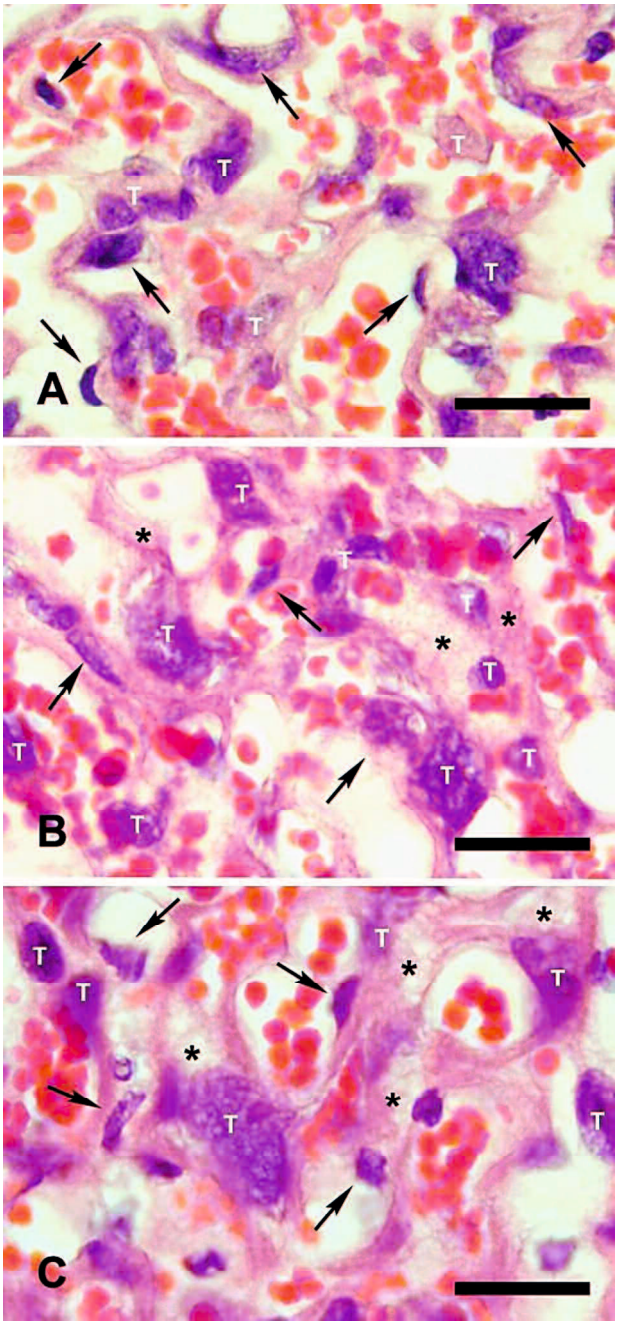

Figure 3. Maternal–fetal barrier in the labyrinthine zone of the placentas from the control mice (A) and from the mice injected with 20-nm (B) and 50-nm gold nanoparticles (C). No severe histopathological lesions are observed. Mild swelling of the cytoplasm (asterisks) of syncytiotrophoblastic cells (T) and endothelial cells (arrows) are observed at the maternal–fetal barrier from the mice injected with 20- and 50-nm gold nanoparticles. Bar = 50 μm.

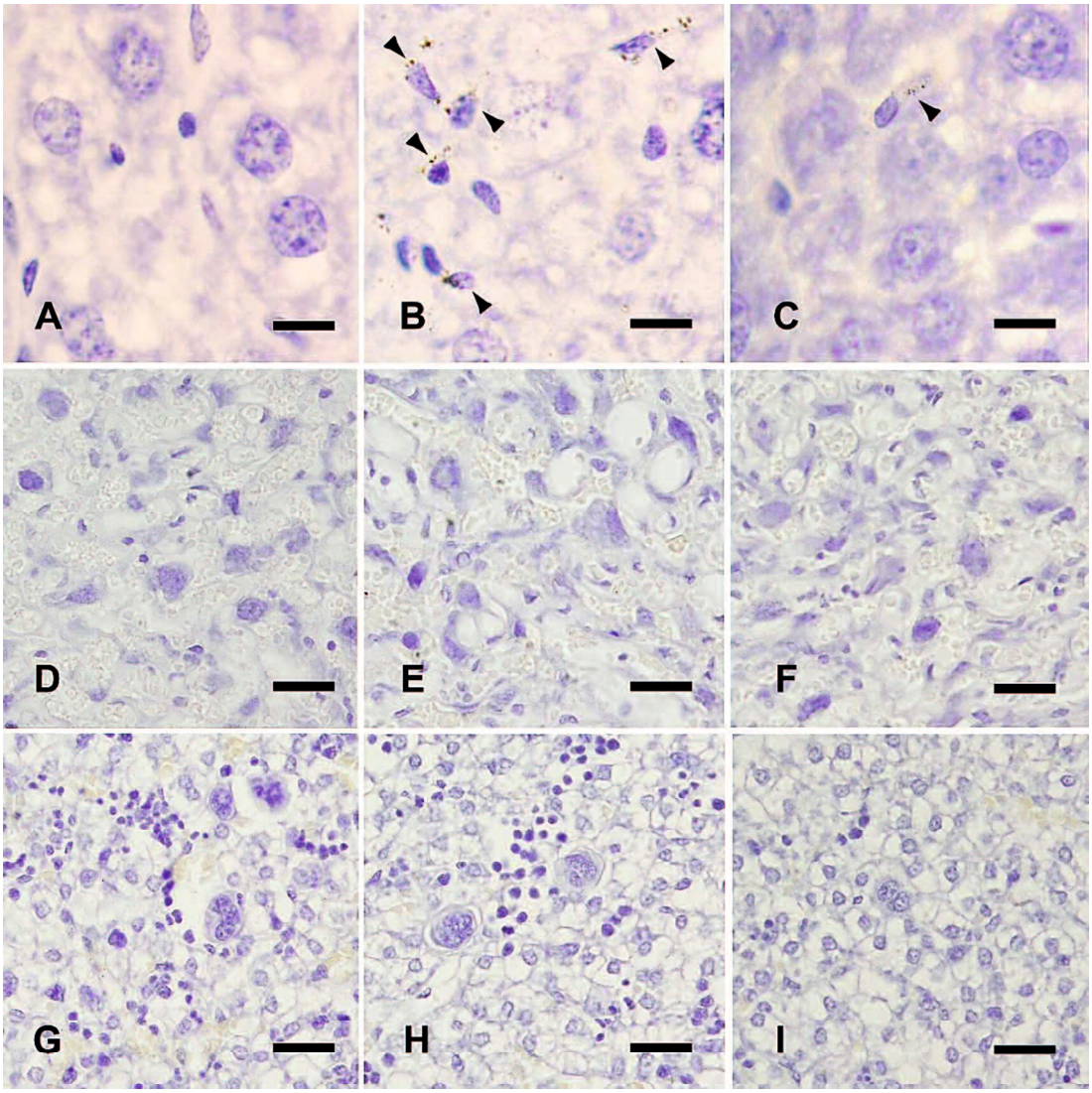

Figure 4. Autometallographic-enhanced gold nanoparticles in maternal livers (A–C), placentas (D–F), and fetal livers (G–I) of the control mice (A, D, and G), the mice intravenously injected with 20-nm gold nanoparticles (B, E, and H) and 50-nm gold nanoparticles (C, F, and I). Gold nanoparticles are demonstrated exclusively in the maternal livers from mice injected with 20- and 50-nm gold nanoparticles. The deposition of gold nanoparticles are shown in Kupffer cells (arrowheads) (B and C). Autometallography shows negative staining in all tissues from the control mice (A, D, and G), placentas (E and F) and fetal livers (H and I) from the mice injected with 20- and 50-nm gold nanoparticles. A–C; bar = 10 μm; D–I; bar = 25 μm

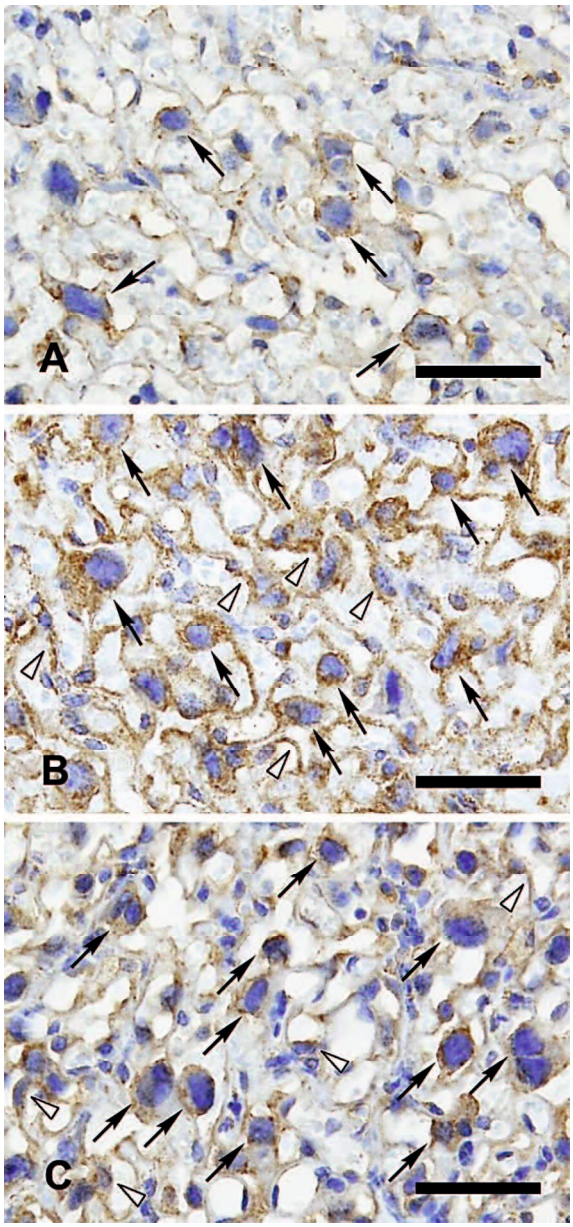

Figure 5. Clathrin immunohistochemistry showing intense positivity in the cytoplasm of trophoblastic cells (arrows) and capillary endothelial cells (white arrowheads) in the maternal–fetal barrier in the labyrinthine zone of placentas from the mice injected with 20-nm (B) and 50-nm (C) gold nanoparticles. Weak positivity is shown in the cytoplasm of trophoblastic cells (arrows) and fetal endothelial cells (white arrowheads) in the maternal–fetal barrier from the control mouse (A). Counterstained with hematoxylin. Bars = 100 μm.

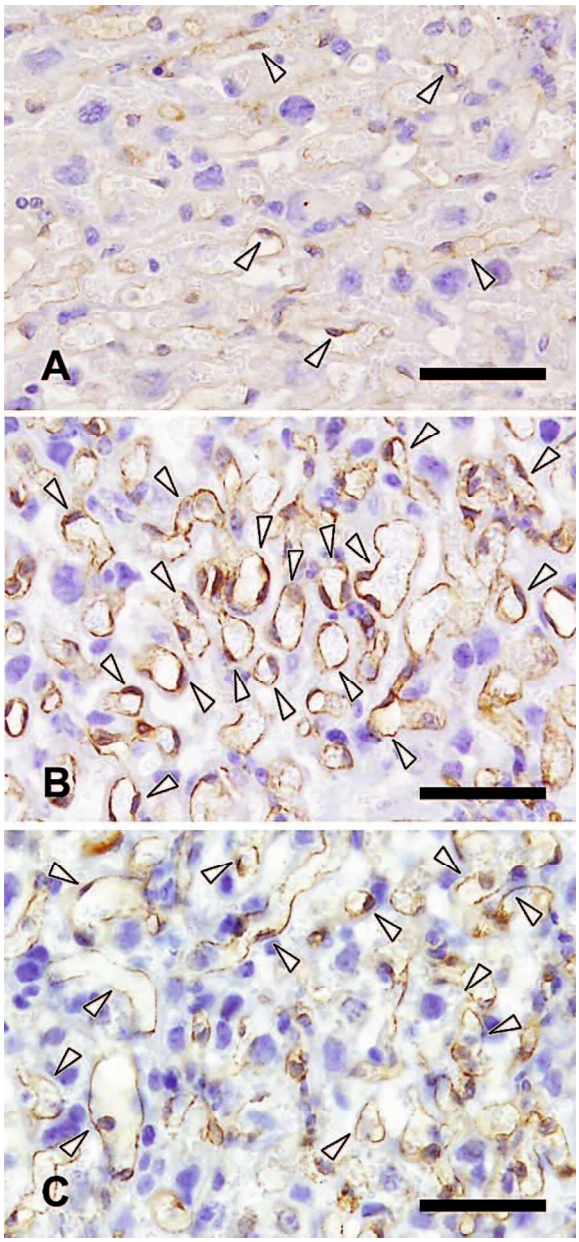

Figure 6. Caveolin-1 immunohistochemistry showing immunopositivity in the cytoplasm of fetal capillary endothelial cells at the maternal–fetal barrier in the labyrinthine zone of the placentas (white arrowheads) from the mice injected with 20-nm (B) and 50-nm (C) gold nanoparticles. Weak positivity is shown in the cytoplasm of fetal endothelial cells in the maternal–fetal barrier from the control mouse (A). Counterstained with hematoxylin. Bars = 100 μm.

Table 2. Positive immunolabeling area in the labyrinthine zone of placentas.

Group	% Positive area[a]	
	Anti-caveolin-1	Anti-clathrin
Control	0.28 ± 0.179	2.73 ± 0.430
20-nm gold NPs	3.57 ± 0.718[b]	12.04 ± 1.495[b]
50-nm gold NPs	2.57 ± 0.926[b]	9.10 ± 1.618[b]

Values are the mean ± standard error.
[a]Positive area (%) of 94,850 μm^2 of 4-μm-thick paraffin sections.
[b]Significantly different from the control group, $P < 0.05$.
NPs = nanoparticles

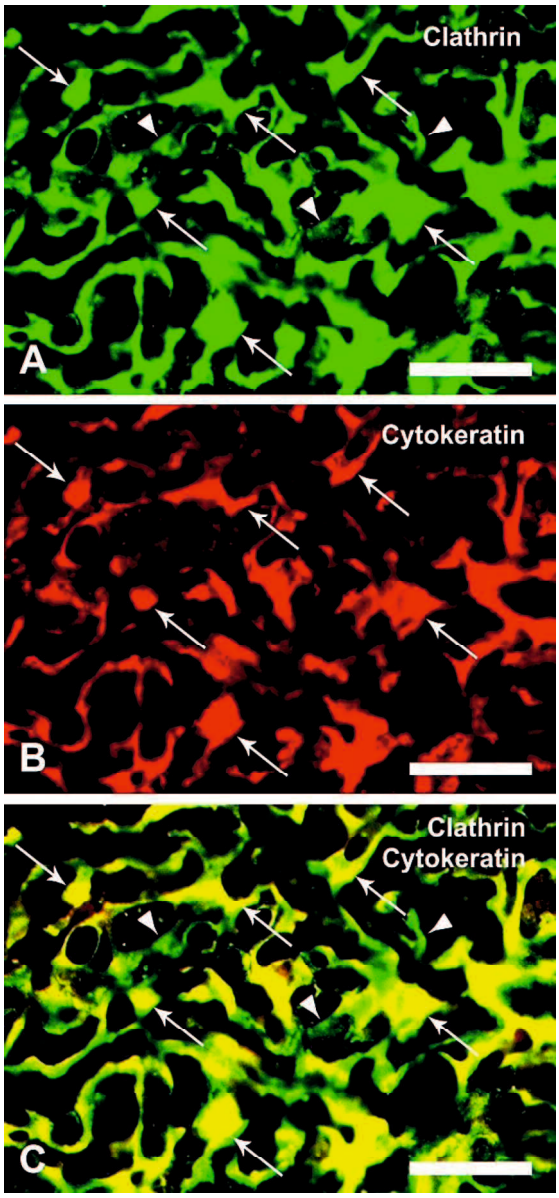

Figure 7. Double immunofluorescence of clathrin and cytokeratin proteins in the labyrinthine zone of mice placenta. Double immunolabeling by antibodies against clathrin as shown by Alexa 488 (green) (A) and cytokeratin as shown by Alexa 555 (red) (B). Merged image with the 2 fluorophores (C). The syncytiotrophoblast layer (white arrows) and fetal vascular wall are strongly labeled with clathrin (white arrowheads) (A). The syncytiotrophoblast layer is exclusively labeled with cytokeratin (white arrows) (B). Co-expression of clathrin and cytokeratin (yellowish) is shown in the syncytiotrophoblast layer (white arrows) (C). Bars = 100 μm.

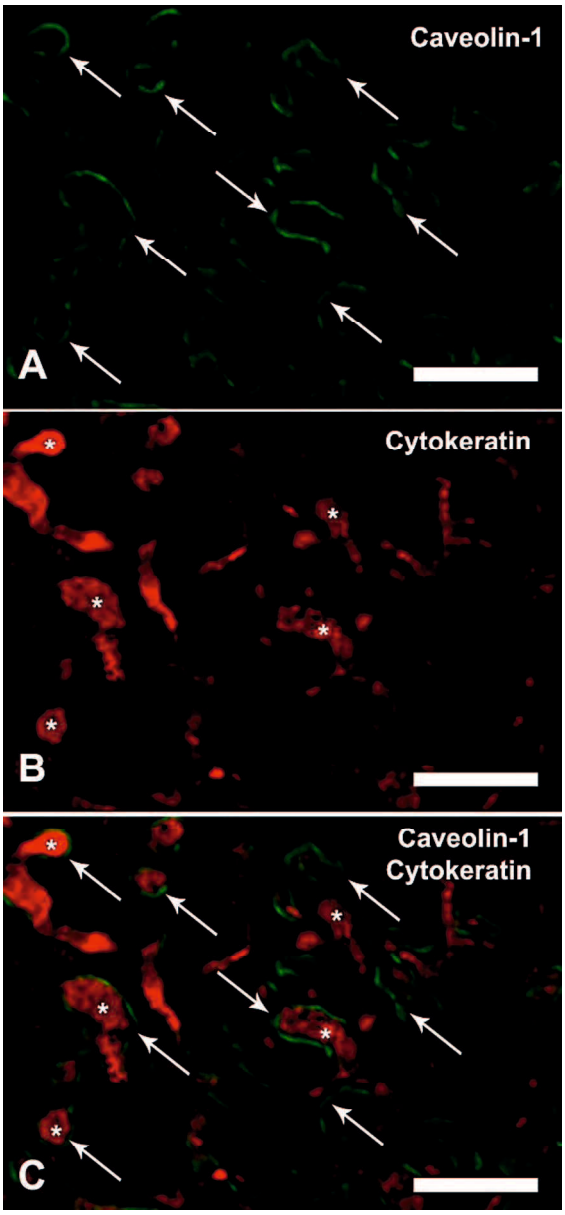

Figure 8. Double immunofluorescence of caveolin-1 and cytokeratin proteins in the labyrinthine zone of mice placenta. Double immunolabeling by antibodies against caveolin-1 as shown by Alexa 488 (green) (A) and cytokeratin as shown by Alexa 555 (red) (B). Merged image with the 2 fluorophores (C). The fetal vascular wall is exclusively labeled with caveolin-1 (white arrows) (A). The syncytiotrophoblast layer is labeled with cytokeratin (white asterisks) (B). Co-expression of caveolin-1 and cytokeratin is not shown in the labyrinthine zone of the placenta. Bars = 100 μm.

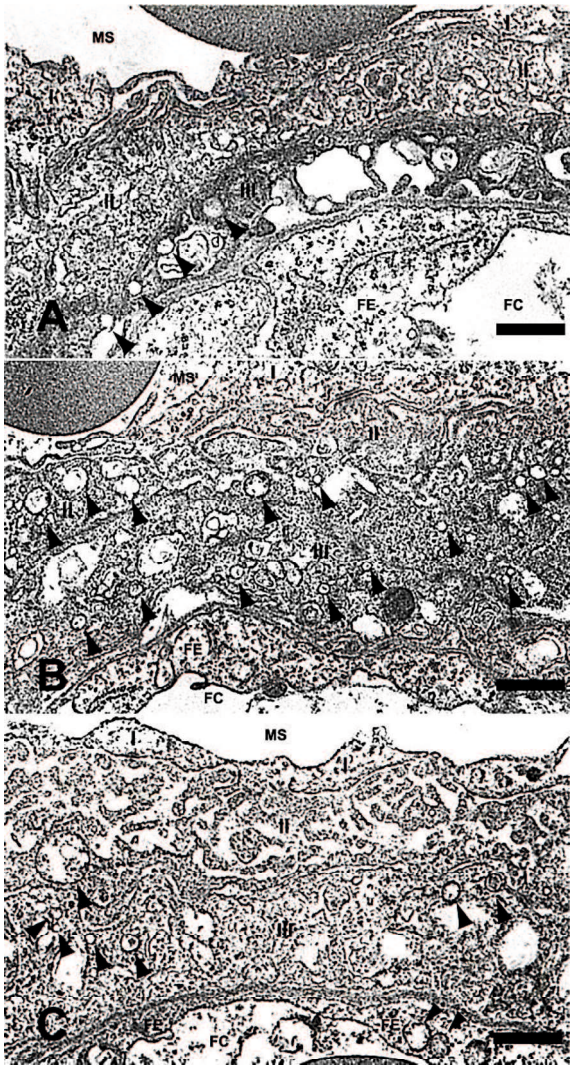

Figure 9. Transmission electron micrographs of maternal–fetal barrier in the labyrinthine zone of the placentas. The placenta from a control mouse consists of 3 syncytiotrophoblast layers with underlying fetal endothelial cells. Numerous microplicae and infolding with a few of vesicle-like structures (arrowheads) are shown in the cytoplasm of syncytiotrophoblast layers II and III in the maternal–fetal barrier from a control mouse (A). Enlargement of the cytoplasm of syncytiotrophoblast layer I, II, III and fetal endothelial cells with an increase in the number of vesicle-like structures (arrowheads) is shown in the maternal–fetal barrier from the mice injected with 20-nm (B) and 50-nm (C) gold nanoparticles. Bar = 0.5 μm. MS = maternal blood sinus, I = syncytiotrophoblast layer I, II = syncytiotrophoblast layer II, III = syncytiotrophoblast layer III, FE = fetal endothelial cell, FC = fetal capillary.

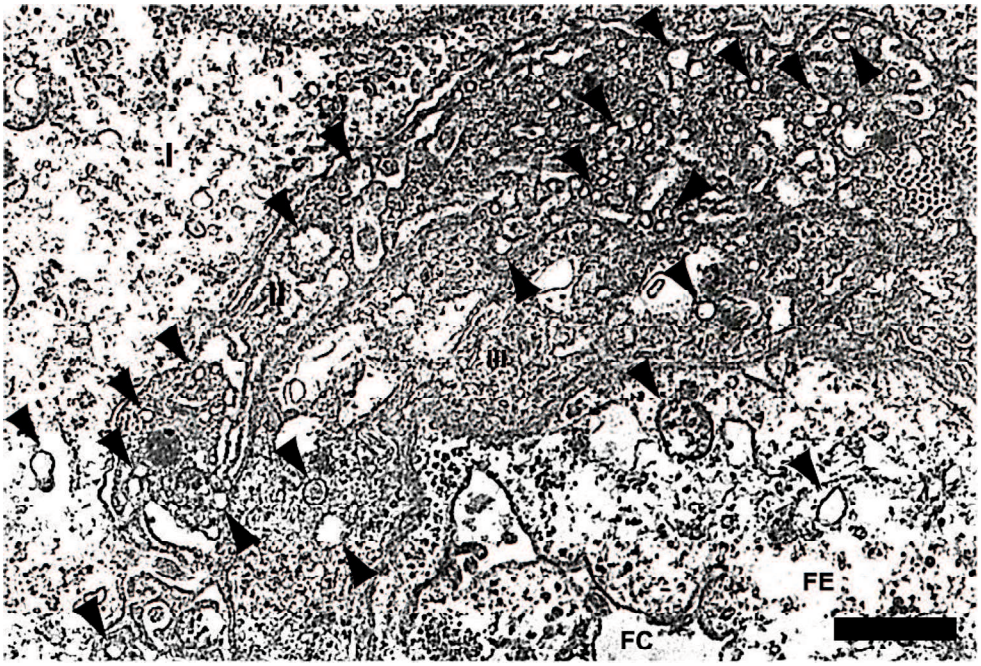

Figure 10. Transmission electron micrograph of the maternal–fetal barrier in the labyrinthine zone of the placenta from the mouse injected with 20-nm gold nanoparticles demonstrating an increase in the number of vesicle-like structures (arrowheads) in the cytoplasm of syncytiotrophoblast layers I, II, III, and fetal endothelial cells. Bar = 0.5 μm. I = syncytiotrophoblast layer I, II = syncytiotrophoblast layer II, III = syncytiotrophoblast layer III, FE = fetal endothelial cell, FC = fetal capillary.

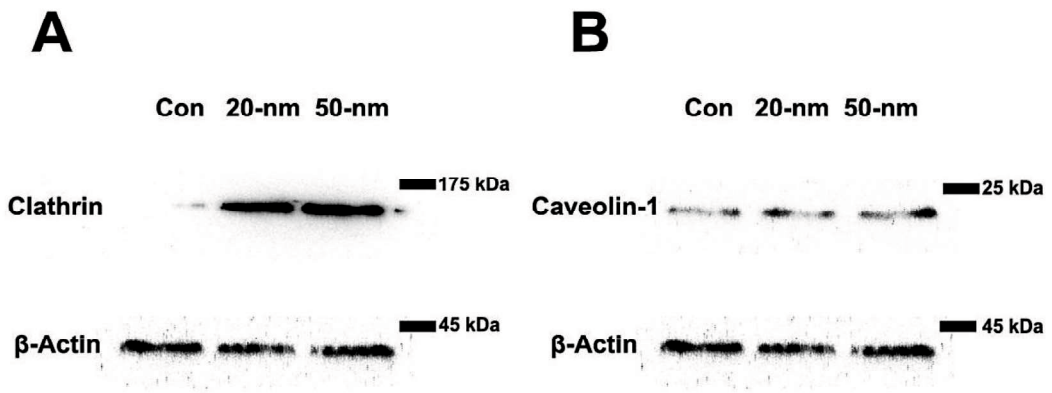

Figure 11. Western blotting demonstrates clathrin and caveolin-1 protein expression in the placental tissues from the pregnant mice. The intensity of clathrin protein band (171 kDa) of placental tissue lysates from the control mice is less than the bands of tissue lysates from the mice injected with 20- and 50-nm gold nanoparticles (A). The intensity of caveolin-1 protein bands is not different between the control mice and the mice treated with 20- and 50-nm gold nanoparticles (B).

Table 3. Integrated density values of the immunoblot band intensity using the image analysis system

Protein	Density of immunoblot band intensity (optical density unit)		
	Control (n = 3)	20-nm gold NPs (n = 3)	50-nm gold NPs (n = 3)
Clathrin	0.20 ± 0.062	1.05 ± 0.029[a]	1.06 ± 0.010[a]
Caveolin-1	1.46 ± 0.167	1.36 ± 0.224	1.55 ± 0.095

Values are the mean ± standard error.
[a]Significantly different from the control group, $P < 0.05$.
NPs = nanoparticles

GENERAL DISCUSSION AND CONCLUSIONS

In the first chapter, the study aimed to demonstrate the precise translocation pathway of the intratracheally instilled nanoparticles during acute pulmonary inflammation caused by Asian sand dust. The exposure to nanoparticles during pulmonary inflammation is a concern because nanoparticles may easily translocate into the systemic circulation and induce adverse effects (Nemmar et al. 2010; Sadauskas et al. 2009a; Saunders 2009). The intratracheal instillation of gold nanoparticles following the instillation of Asian sand dust was carried out for examination of the translocation pathway of gold nanoparticles after pulmonary injury induced by Asian Sand dust particles. Histopathological and ultrastructural findings of lungs from mice treated with Asian sand particles and gold nanoparticles showed severe injury to the alveolar wall structure in contrast to lungs from mice treated with gold nanoparticles alone. These findings suggest that Asian sand particles may have severe toxic effects on the structure of the air–blood barrier (Hiyoshi et al. 2005; Ichinose et al. 2005; Naota et al. 2010). An intense expression of proinflammatory cytokines and oxidative stress markers was found in alveolar macrophages, type I and II alveolar epithelial cells, and endothelial cells at the alveolar walls of lungs from mice instilled with Asian sand particles and gold nanoparticles. It suggested that the release of proinflammatory cytokines and the generation of oxidative stress may be involved in the pulmonary destruction induced by Asian sand particles (Figure 1) (Hamilton et al. 2008; Ichinose et al. 2005; Meng and Zhang 2006; Naota et al. 2010). Electron microscopy also demonstrated a ruffling of the surface of type I epithelial cells and an increase in the number of endocytic vesicles in both type I alveolar epithelial cells and endothelial cells at the alveolar wall of both lungs from mice instilled with gold nanoparticles alone and lungs from mice instilled with Asian sand dust and gold nanoparticles. In addition, an increased number of endocytic vesicles containing gold nanoparticles was also found in

the alveolar epithelial cells and the endothelial cells. Endocytosis was shown to play an important role in the internalization of many nanoparticles, including gold nanoparticles (Figure 2) (Shukla et al. 2005). These findings suggest that the translocation by the endocytotic process of the exposed nanoparticles may be enhanced in the lung tissues with acute inflammatory changes (Figure 3).

In the second chapter, the aim of the study was to determine the possible translocation mechanism of gold nanoparticles across the maternal–fetal (placental) barrier of mice. The intravenous administrations of 20- and 50-nm gold nanoparticles to pregnant mice were conducted for examination of the translocation pathway at the maternal–fetal barrier. The present study on the mouse placentas demonstrated an increase in the number of endocytic vesicles in the cytoplasm of syncytiotrophoblasts and fetal endothelial cells by electron microscopy, suggesting that endocytosis was upregulated in the maternal–fetal barrier after injection of gold nanoparticles. Endocytotic processes may play an important role for the translocation of nanoparticles at the maternal–fetal barrier (Figure 4). Clathrin immunohistochemistry showed an increase of intense positivity in the endocytic vesicles of both syncytiotrophoblasts and fetal endothelial cells, while caveolin-1 immunohistochemistry was observed exclusively in the fetal endothelium after the administration of gold nanoparticles. Double immunofluorescence revealed the presence of clathrin and caveolin-1 in the maternal–fetal barrier after intravenous injection with gold nanoparticles. Clathrin was demonstrated in the syncytiotrophoblasts and fetal capillary endothelium. In contrast, caveolin-1 was demonstrated in the vasculatures, especially in the fetal capillary endothelium. Clathrin-mediated endocytosis was previously described in the cytoplasm of syncytiotrophoblasts of the mouse placenta (Lambot et al. 2006). Clathrin-mediated endocytosis is involved in the recycling of albumin in the term placenta, neurotransmitter transport, and the internalization of several viruses (Lambot et al. 2006; McMahon and

Boucrot 2011; Mousavi et al. 2004). Immunoblot analysis showed an increase in clathrin protein expression in the placental tissues from mice administered with gold nanoparticles, suggesting that gold nanoparticle administration upregulated clathrin expression in the placenta and clathrin-mediated endocytosis may be one of the endocytotic pathways of the translocation of nanoparticles in the maternal–fetal barrier. Apart from clathrin-mediated endocytosis, caveolae-mediated endocytosis is considered to be another pathway for the translocation of nanoparticles in the biological barrier (Naota et al. 2013). Caveolin-1 protein may play a role in the regulation of caveolar invagination and the formation of caveolae, which is one form of the endocytic vesicle (Linton et al. 2003; Nabi and Le 2003; Pelkmans and Helenius 2002; Rothberg et al. 1992). However, immunoblotting showed no difference in the amount of caveolin-1 expression between the control mice and the mice administered with gold nanoparticles, suggesting the possible re-assembly of caveolin-1 protein from the cytosol to the caveolae structure after the exposure to nanoparticles.

In summary, the studies of two chapters showed detailed about possible translocation pathway of nanoparticles in specific health conditions (Figure 5). The studies focused on the biological barriers, including air–blood barrier in lung and maternal–fetal barrier in placenta. The evaluation of the potential adverse health effect responses resulting from exposure to nanoparticles is particularly important, especially for susceptible subpopulations, e.g. unhealthy people, pregnant women, and their fetuses. The study on the translocation pathway of nanoparticles in the biological barriers may be critical to assess the risks of the uses of nanoparticle-containing products. Moreover, the results may be useful in predicting the biodistribution and toxicity of nanoparticles in the subpopulation comparing with the healthy people.

In conclusion, the translocation of nanoparticles during specific conditions was demonstrated in the present studies (Figure 5). However, the current studies failed to detect

the signs of nanoparticle toxicity in the systemic organs. Further study with prolonged duration, different kinds of nanoparticles and sensitive techniques for the detection of nanoparticles is required to ascertain whether exposed nanoparticles may have a chance to cause serious toxicity in the subpopulation.

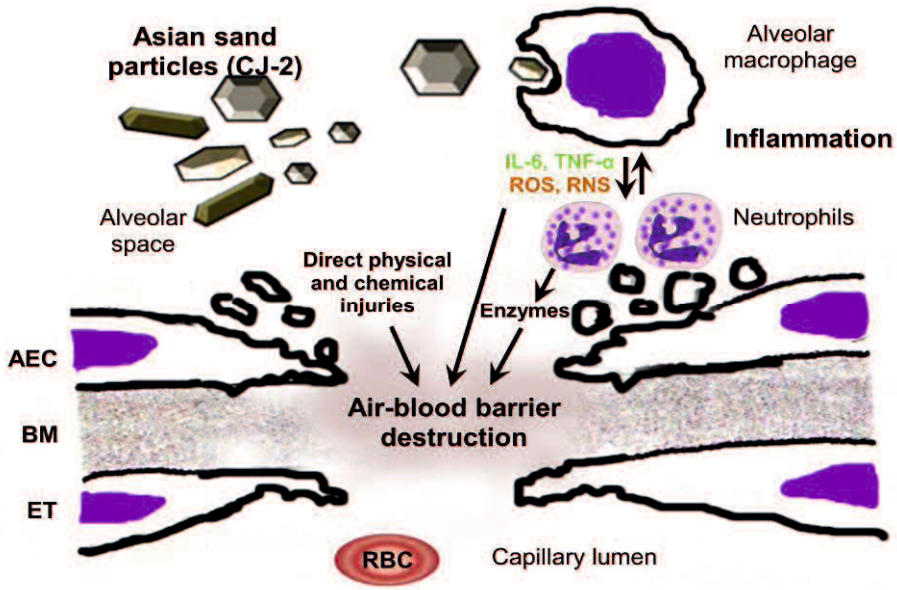

Figure 1. Schematic diagram shows the possible mechanisms of the air–blood barrier injury induced by Asian sand dust. Direct physical and chemical injuries by the Asian sand particles, the release of proinflammatory cytokines and the generation of oxidative stress by activated alveolar macrophages, and the migration of neutrophils may be involved in the air–blood barrier destruction induced by Asian sand dust. AEC = alveolar epithelial cell, BM = basement membrane, ET = endothelial cell, ROS = reactive oxygen species, RNS = reactive nitrogen species.

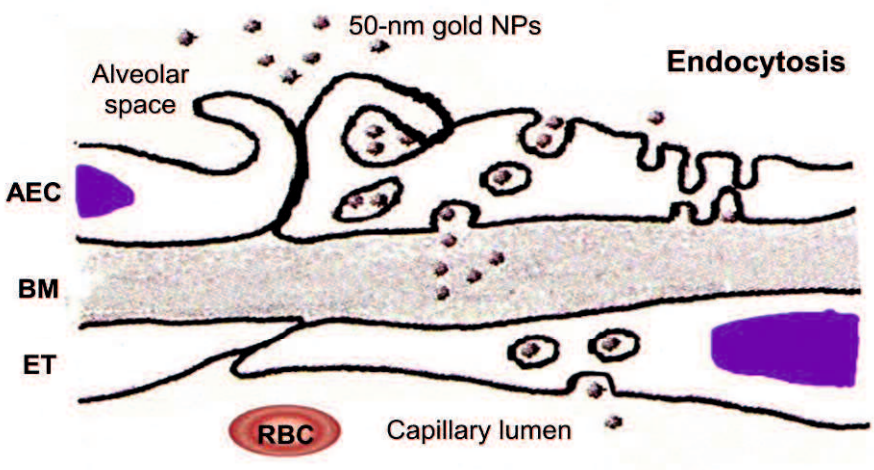

Figure 2. Schematic diagram shows the possible translocation pathway of gold nanoparticles in the air–blood barrier by endocytosis in the physiological condition. AEC = alveolar epithelial cell, BM = basement membrane, ET = endothelial cell.

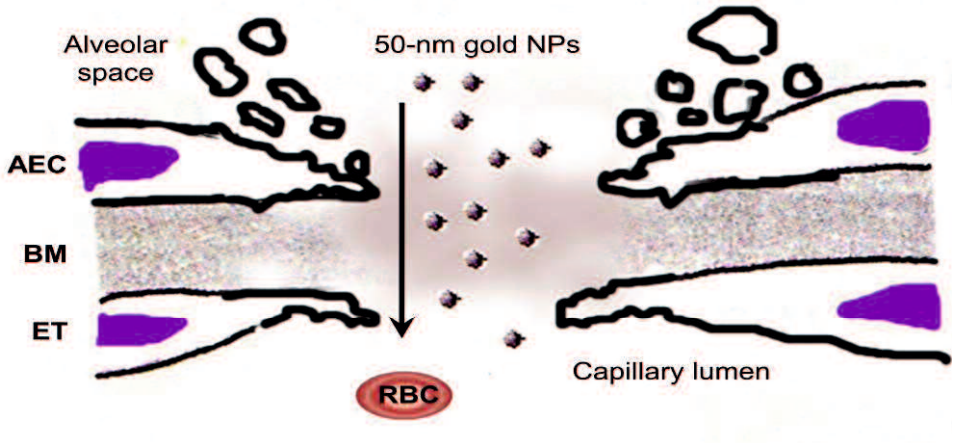

Figure 3. Schematic diagram shows the possible translocation pathway of gold nanoparticles across the destructive air–blood barrier induced by Asian sand particles. AEC = alveolar epithelial cell, BM = basement membrane, ET = endothelial cell.

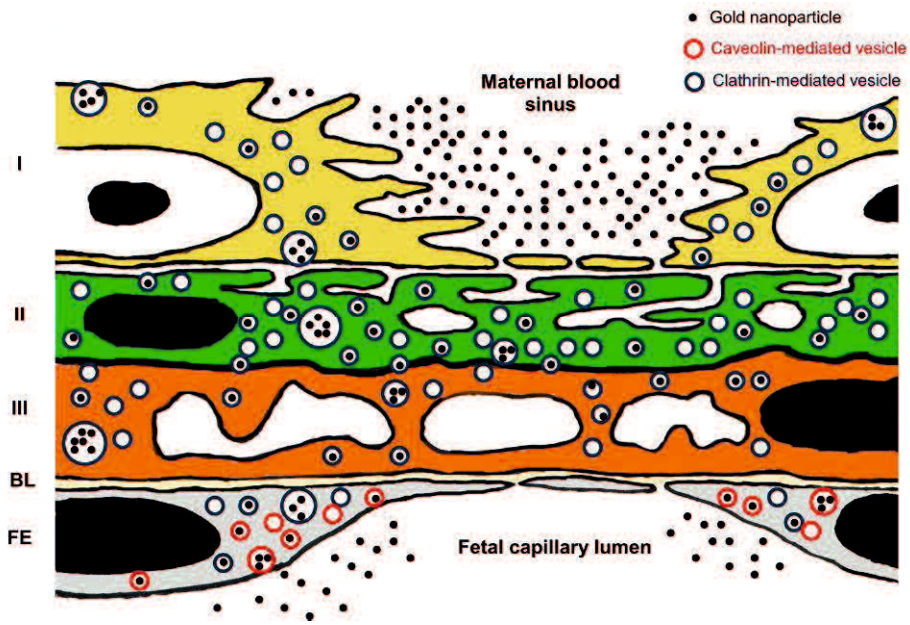

Figure 4. The schematic diagram shows the possible translocation pathway of gold nanoparticles at the maternal–fetal barrier in the labyrinthine zone of placenta. Clathrin-mediated endocytosis is demonstrated in the syncytiotrophoblasts and fetal vascular endothelium. In contrast, caveolae-mediated endocytosis is observed exclusively in the fetal endothelium. I = syncytiotrophoblast layer I, II = syncytiotrophoblast layer II, III = syncytiotrophoblast layer III, BL = basal lamina, FE = fetal endothelial cell.

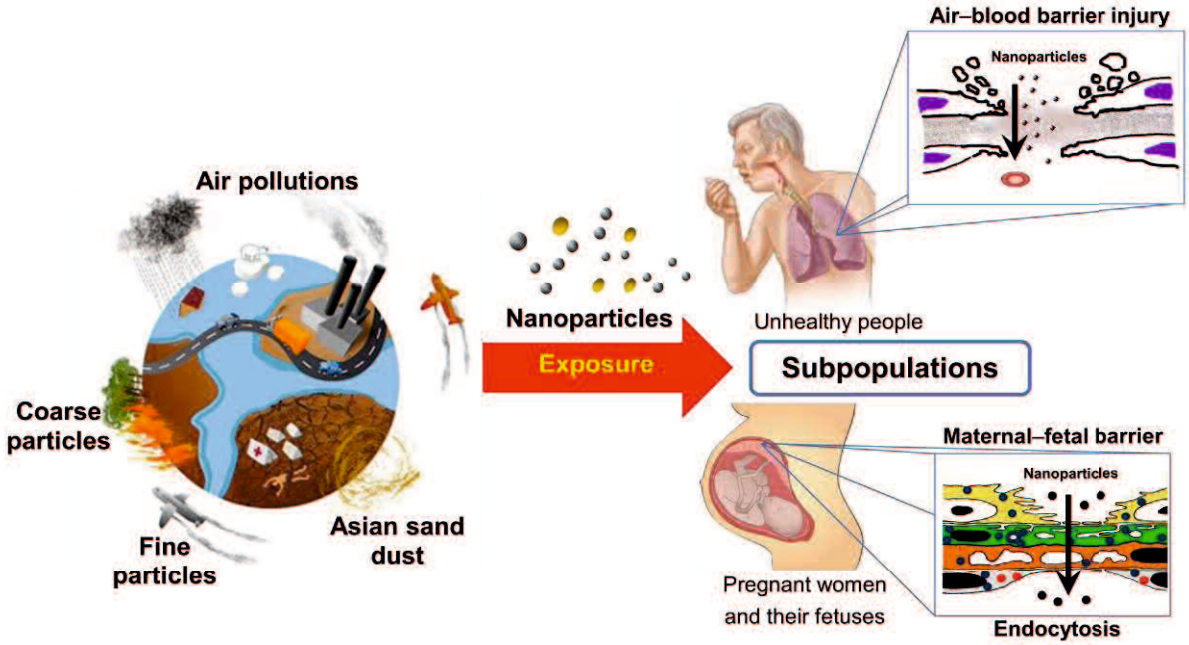

Figure 5. Schematic diagram shows the possible risk of the co-exposure of ambient pollutions and nanoparticles in the subpopulations, including unhealthy people, pregnant women, and their fetuses. The exposed nanoparticles may be increased translocation across the physiological barrier injuries induced by the ambient pollution, e.g. air–blood barrier injury induced by Asian sand dust. In addition, nanoparticles may be capable to transfer across the maternal–fetal barrier by endocytosis during pregnant period.

ACKNOWLEDGMENTS

The research for this Ph.D. thesis was carried out at Department of Veterinary Pathology, Faculty of Agriculture, Tottori University. My sincere appreciated and gratitude belong to Professor. Dr. Akinori Shimada (Laboratory of Pathology, School of Life and Environmental Science, Azabu University) for his firm guidance, pragmatic touch throughout this work and for his kindness introducing me to Japan through the Japan Government Scholarship (Monbukagakusho). I am deeply grateful to my supervisor Professor Dr. Takehito Morita (Tottori University) for his guidance and his dedication and encouragement during this work. I also thank my co-supervisor Professor Dr. Toshiharu Hayashi (Yamaguchi University) for his expert advice and encouragement during the whole course of this thesis work. I also want to thank all the other co-authors for their contributions in this work.

I warmly thank my collaborators in the particulate matter (PM) team, Dr. Misaki Naota, Ms. Yuko Yamamoto, Ms. Shizuka Shiotsu, Ms. Yukari Kohara, Mr. Yoshimi Kobayashi, and Ms. Mai Nemoto for their fruitful collaboration. I would like to thank Assistant Professor Dr. Theerayuth Kaewamatawong (Department of Veterinary Pathology, Chulalongkorn University, Bangkok Thailand) and Mr. Masashi Sakurai (Department of Veterinary Pathology, Tottori University) for giving excellent assistance in the study. I would like to thank Professor Dr. Tatsuya Hasegawa for his kindness help in ICP-MS method. I also would like to thank Ms. Eiko Kawahara and Ms. Miho Taniguchi for their excellent assistance in electron microscopy at Tottori University and Professor Dr. Yoshiaki Yamano and Associated Professor Dr. Atsushi Asano (Department of Veterinary Biochemistry, Tottori University) and Associated Professor Dr. Hiroichi Ozaki (Department of Veterinary Microbiology, Tottori University) for their technical assistance in Western blotting. I am grateful to the whole students of Department of Veterinary Pathology, Tottori University for

their continuous support and assistance. I wish to express my heartfelt gratitude to all my friends in Thailand and Japan for their relaxing company and for giving me chances my mind off the work.

Finally, I am especially grateful to my family for their never-ending love, the encouragement given to me, and for supporting me in all my efforts by over the years.

REFERENCES

Aumailley, M., and Smyth, N. (1998). The role of laminins in basement membrane function. *J Anat* **193**, 1–21.

Austin, C. A., Umbreit, T. H., Brown, K. M., Barber, D. S., Dair, B. J., Francke-Carroll, S., Feswick, A., Saint-Louis, M. A., Hikawa, H., Siebein, K. N. and Goering, P. L. (2011). Distribution of silver nanoparticles in pregnant mice and developing embryos. *Nanotoxicolgy* **6**, 912–922.

Balasubramanian, S. K., Jittiwat, J., Manikandan, J., Ong, C., Yu, L. E. and Ong, W. (2010). Biodistribution of gold nanoparticles and gene expression changes in the liver and spleen after intravenous administration in rats. *Biomaterials* **31**, 2034–2042.

Bell, M. and Davis, D. (2001). Reassessment of the lethal London fog of 1952: novel indications of acute and chronic consequences of acute exposure to air pollution. *Envirn Health Perspect* **109**, 389–394.

Bettmer, J., Bayón, M. M., Encinar, J. R., Sánchez, M. L. F., de la Campa, M. R. F., and Medal, A. S. (2009). The emerging role of ICP-MS in proteomic analysis. *J Proteomics* **72**, 984–1005.

Bhabra, G., Sood, A., Fisher, B., Cartwright, L., Saunders, M., Evans, W. H., Surprenant, A., Lopez-Castejon, G., Mann, S., Davis, S. A., Hails, L. A., Ingham, E., Verkade, P., Lane, J., Heesom, K., Newson, R., and Case, C. P. (2009). Nanoparticles can cause DNA damage across a cellular barrier. *Nature Nanotechnol* **4**, 876–883.

Braydich-Stolle, L., Hussain, S., Schlager. J. J., and Hofmann, M. C. (2005). *In vitro* cytotoxicity of nanoparticles in mammalian germline stem cells. *Toxicol Sci* **88**, 412–419.

Bryne, S., Ahenkorah, J., Hottor, B., Lockwood, C. and Ockleford, C. D. (2007). Immuno-electron microscopic localization of caveolin 1 in human placenta. *Immunobiol* **212**, 39–46.

Buerki-Thurnherr, T., von Mandach, U. and Wick, P. (2012). Knocking at the door of the unborn child: engineered nanoparticles at the human placental barrier. *Swiss Med Wkly* **142**, w13559.

Cartwright, L., Poulsen, M. S., Nielsen, H. M., Pojana, G., Knudsen, L. E., Saunders, M. and Rytting, E. (2012). In vitro placental model optimization for nanoparticle transport studies. *Int J Nanomedicine* **7**, 497–510.

Chang, S., Chou, C. C., Chen, W., and Lee, C. (2010). Asian dust and pollution transport-A comprehensive observation in the downwind Taiwan in 2006. *Atmos Res* **95**, 19–31.

Chen, M. and von Mikecz, A. (2005). Formation of nucleoplasmic protein aggregates impairs nuclear function in response to SiO_2 nanoparticles. *Exp Cell Res* **305**, 51–62.

Chen, Y., Sheen, P., Chen, E., Liu, Y., Wu, T., and Yang, C. (2004). Effects of Asian dust storm events on daily mortality in Taipei, Taiwan. *Environ Res* **95**, 151–155.

Cho, W., Choi, M., Han, B. S., Cho, M., Oh, J., Park, K., Kim, S. J., Kim, S. H., and Jeong, J. (2007). Inflammatory mediators induced by intratracheal instillation of ultrafine amorphous silica particles. *Toxicol Lett* **175**, 24-33.

Chu, M., Wu, Q., Yang, H., Yuan, R., Hou, S., Yang, Y., Zou, Y., Xu, S., Xu, K., Ji, A., and Sheng, L. (2010). Transfer of quantum dots from pregnant mice to pups across the placental barrier. *Small* **6**, 321–328.

Chung, Y., and Yoon, M. (1996). On the occurrence of yellow sand and atmospheric loadings. *Atmos Environ* **30**, 2387–2397.

Conner, S. D., and Schmid, S. L. (2003). Regulated portals of entry into the cell. *Nature* **422**, 37–44.

Cox, B., Kotlyar, M., Evangelou, A. I., Ignatchenko, V., Ignatchenko, A., Whiteley, K., Jurisica, I, Adamson, S. L., Rossant, J., and Kislinger, T. (2009). Comparative systems biology of human and mouse as a tool to guide the modeling of human placental pathology. *Mol Syst Biol* **5**, 279.

Danscher, G. (1984). Autometallography. a new technique for light and electron microscopic visualization of metals in biological tissues (gold, silver, metal sulphides). *Histochem* **81**, 331–335.

Danscher, G. and Stoltenberg, M. (2006). Silver enhancement of quantum dots resulting from (1) metabolism of toxic metals in animals and humans, (2) in vivo, in vitro and immersion created zinc-sulphur/zinc-selenium nanocrystals, (3) metal ions liberated from metal implants and particles. *Prog Histochem Cytochem* **41**, 57–139.

De Jong, W. H., Hagens, W. I., Krystek, P., Burger, M. C., Sips, A. J. A. M., and Geertsma, R. E. (2008). Particles size-dependent organ distribution of gold nanoparticles after intravenous admistration. *Biomaterials* **29**, 1912–1919.

Elsaesser, A. and Howard, V. (2012). Toxicology of nanoparticles. *Adv Drug Delivery Rev* **64**, 129–137.

Ema, M., Kobayashi, N., Naya, M., Hanai, S. and Nakanishi, J. (2010). Reproductive and developmental toxicity studies of manufactured nanomaterials. *Reprod Toxicol* **30**, 343–352.

European commission. (1997). Ambient air pollution by particulate matter. European commission. Available from http://ec.europa.eu/environment/air/pdf/pp_pm.pdf.

Fedulov, A. V., Leme, A., Yang, Z., Dahl, M., Lim, R., Mariani, T. J., and Kobzik, L. (2008). Pulmonary exposure to particles during pregnancy causes increased neonatal asthma susceptibility. *Am J Respir Mol Biol* **38**, 57–67.

Furukawa, S., Hayashi, S., Usuda, K., Abe, M., Hagio, S. and Ogawa, I. (2011). Toxicological pathology in the rat placenta. *J Toxicol Pathol* **24**, 95–111.

Furuyama, A., Kanno, S., Kobayashi, T., and Hirano, S. (2009). Extrapulmonary translocation of intratracheally instilled fine and ultrafine particles via direct and alveolar macrophage-associated routes. *Arch Toxicol* **83**, 429–437.

Hamilton, J. R. F., Thakur, S. A., and Holian, A. (2008). Silica binding and toxicity in alveolar macrophages. *Free Radical Bio Med* **44**, 1246–1258.

Hiyoshi, K., Ichinose, T., Sadakane, K., Takano, H., Nishikawa, M., Mori, I., Yanagisawa, R., Yoshida, S., Kumagai, Y., Tomura, S., and Shibamoto, T. (2005). Asian sand dust enhances ovalbumin-induced eosinophil recruitment in the alveoli and airway of mice. *Environ Res* **99**, 361–368.

Hong, Y., Pan, X., Kim, S., Park, K., Park, E., Jin, X., Yi, S., Kim, Y., Park, C., Song, S., and Kim, H. (2010). Asian dust storm and pulmonary function of school children in Seoul. *Sci Total Environ* **408**, 754–759.

Husar, R. B., Tratt, D. M., Schichtel, B. A., Falke, S. R., Li, F., Jaffe, D., Gassó, S., Gill, T., Laulainen, N. S., Lu, F., Reheis, M. C., Chun, Y., Westphal, D., Holben, B. N., Gueymard, C., McKendry, I., Kuring, N., Feldman, G. C., McClain, C., Frouin, R. J., Merrill, J., DuBois, D., Vignola, F., Murayama, T., Nickovic, S., Wilson, W. E., Sassen, K., Sugimoto, N., and Walm, W. C. (2001). Asian dust events of April 1998. J *Geophys Res* **106**, 18317–18330.

Hussain, S., Boland, S., Baeza-Squiban, A., Hamel, R., Thomassen, L. C. J., Martens, J. A., Billon-Galland, M. A., Fleury-Feith, J., Moisan, F., Pairon, J., and Marano, F. (2009). Oxidative stress and proinflammatory effects of carbon black and titanium dioxide nanoparticles: role of particle surface area and internalized amount. *Toxicology* **260**, 142–149.

Ichinose, T., Nishikawa, M., Takano, H., Sera, N., Sadakane, K., Mori, I., Yanagisawa, R., Oda, T., Tamura, H., Hiyoshi, K., Quan, H., Tomura, S., and Shibamoto, T. (2005). Pulmonary toxicity induced by intratracheal instillation of Asian yellow dust (Kosa) in mice. *Environ Toxicol Pharmacol* **20**, 48–56.

Inoue, H., Shimada, A., Kaewamatawong, T., Naota, M., Morita, T., Ohta, Y., Inoue, K., and Takano, H. (2009). Ultrastructural changes of the air blood barrier in mice after intratracheal instillation of lipopolysaccharide and ultra carbon black particles. *Exp Toxicol Pathol* **61**, 51–58.

Inoue, K., Takano, H., Yanagisawa, R., Hirano, S., Kobayashi, T., Fujitani, Y., Shimada, A., and Yoshikawa, T. (2007). Effects of inhaled nanoparticles on acute lung injury induced by lipopolysaccharide in mice. *Toxicology* **238**, 99–110.

Kaewamatawong, T., Kawamura, N., Okajima, M., Sawada, M., Morita, T., and Shimada, A. (2005). Acute pulmonary toxicity caused by exposure to colloidal silica: particle size dependent pathological changes in mice. *Toxicol Pathol* **33**, 745–751.

Keelan, J. A. (2011). Nanoparticles versus the placenta. *Nanotoxicology* **6**, 263–264.

Khan, H. M., Khan, M. Y. and Minhas, L. A. (2011). Histological study of the developing mouse placenta. *J Rawal Med Coll* **15**, 116–119.

Kim, S., Yoon, S., Kim, J., Kang, J., and Sugimoto, N. (2010). Asian dust event observed in Seoul, Korea, during 29-31 May 2008: analysis of transport and vertical distribution of dust particles from lidar and surface measurements. *Sci Total Environ* **408**, 1707–1718.

Kirby, D. R. S., and Bradbury, S. (1965). The hemo-chorial mouse placenta. *Anat Rec* **152**, 279–282.

Komatsu, T., Tabata, M., Kubo-Irie, M., Shimizu, T., Suzuki, K., Nihei, Y., and Takeda, K. (2008). The effects of nanoparticles on mouse testis Leydig cells *in vitro*. *Toxicol in Vitro* **22**, 1825–1831.

Kulvietis, V., Zalgeviciene, V., Didzipetriene, J. and Rotomskis, R. (2011). Transport of nanoparticles through the placental barrier. *Tohoku J Exp Med* **225**, 225–234.

Laks, D., De Oliveira, R. C., De André, P. A., Macchione, M., Lemos, M., Faffe, D., Saldiva, P. H. N., and Zin, W. A. (2008). Composition of diesel particles influences acute pulmonary toxicity: an experimental study in mice. *Inhal Toxicol* **20**, 1037–1042.

Lambot, N., Lybaert, P., Boom, A., Delogne-Desnoeck, J., Vanbellinghen, A. M., Graff, G., Lebrun, P. and Meuris, S. (2006). Evidence for a clathrin-mediated recycling of albumin in human term placenta. *Biol Reprod* **74**, 90–97.

Lasagna-Reeves, C., Gonzalez-Romero, D., Barria, M. A., Olmedo, I., Clos, A., Ramanujam, V. M. S., Urayama, A., Vergara, L., Kogan, M. J. and Soto, C. (2010). Bioaccumulation and toxicity of gold nanoparticles after repeated administration in mice. *Biochem Biophy Res Com* **393**, 649–655.

Le Roy, C., and Wrana, J. L. (2005). Clathrin- and non-clathrin- mediated endocytic regulation of cell signalling. *Nature Reviews* **6**, 112–126.

Li, N., Xia, T., and Nel, A. E. (2008). The role of oxidative stress in ambient particulate matter-induced lung diseases and its implications in the toxicity of engineered nanoparticles. *Free Radical Bio Med* **44**, 1689–1699.

Linton, E. A., Rodriguez-Linares, B., Rashid-Doubell, F., Ferguson, D. J. P. and Redman, C. W. G. (2003). Caveolae and caveolin-1 in human term villous trophoblast. *Placenta* **24**, 745–757.

Lipka, J., Semmler-Behnke, M., Sperling, R. A., Wenk, A., Takenaka, S., Schlen, C., Kissel, T., Parak, W. J., and Kreyling, W. G. (2010). Biodistribution of PEG-modified gold nanoparticles following intratracheal instillation and intravenous injection. *Biomaterials* **31**, 6574–6581.

Lyden, T. W., Anderson, C. L. and Robinson, J. M. (2002). The endothelium but not the synctiotrophoblast of human placenta expresses caveolae. *Placenta* **23**, 640–652.

Maki, T., Susuki, S., Kobayashi, F., Kakikawa, M., Tobo, Y., Yamada, M., Higashi, T., Matsuki, A., Hong, C., Hasegawa, H., and Iwasaka, Y. (2010). Phylogenetic analysis of atmospheric halotolerant bacterial communities at high altitude in an Asian dust (KOSA) arrival region, Suzu city. *Sci Total Environ* **408**, 4556–4562.

McMahon, H. T., and Boucrot, E. (2011). Molecular mechanism and physiological functions of clathrin-mediated endocytosis. *Nature Reviews* **12**, 517–533.

Mehrabi, M. and Wilson, R. (2007). Intercalating gold nanoparticles as universal labels for DNA detection. *Small* **3**, 1491–1495.

Meng, Z., and Lu, B. (2007). Dust events as a risk factor for daily hospitalization for respiratory and cardiovascular diseases in Minqin, China. *Atmos Environ* **41**, 7048–7058.

Meng, Z., and Zhang, Q. (2006). Oxidative stress of dust storm fine particles instillation on lungs, hearts and livers of rats. *Environ Toxicol Pharmacol* **22**, 277–282.

Mohanty, S., Anderson, C. L. and Robinson, J. M. (2010). The expression of caveolin-1 and the distribution of caveolae in the murine placenta and yolk sac: parallels to the human placenta. *Placenta* **31**, 144–150.

Mori, I., Nishikawa, M., Tanimura, T., and Quan, H. (2003). Change in size distribution and chemical composition of kosa (Asian dust) aerosol during long-range transport. *Atmos Environ* **37**, 4253–4263.

Mousavi, S. A., Malerød, L., Berg, T. and Kjeken, R. (2004). Clathrin-dependent endocytosis. *Biochem J* **377**, 1–6.

Myllynen, P. K., Loughran, M. J., Howard, C. V., Sormunen, R., Walsh, A. A. and Vähäkangas, K. H. (2008). Kinetics of gold nanoparticles in the human placenta. *Reprod Toxicol* **26**, 130–137.

Myojo, T., Ogami, A., Oyabu, T., Morimoto, Y., Hirohashi, M., Murakami, M., Nishi, K., Kadoya, C., and Tanaka, I. (2010). Risk assessment of airborne fine particles and nanoparticles. *Adv Powder Technol* **21**, 507–512.

Nabi, I. R. and Le, P. U. (2003). Caveolae/raft-dependent endocytosis. *J Cell Biol* **161**, 673–677.

Naota, M., Mukayama, T., Shimada, A., Yoshida, A., Morita, T., Inoue, K., and Takano, H. (2010). Pathological study of acute pulmonary toxicity induced by intratracheally instilled Asian sand dust (Kosa). *Toxicol Pathol* **38**, 1099–1110.

Naota, M., Shimada, A., Morita, T., Yamamoto, Y., Inoue, K. and Takano, H. (2013). Caveolae-mediated endocytosis of intratracheally instilled gold colloid nanoparticles at the air–blood barrier in mice. *Toxicol Pathol* **41**, 487–496.

Nemmar, A., Al-Salam, S., Zia, S., Dhanasekaran, S., Shudadevi, M., and Ali, B. H. (2010). Time-course effects of systemically administered diesel exhaust particles in rats. *Toxicol Lett* **194**, 56–65.

Nishikawa, M., Quan, H., and Morita, M. (2000). Preparation and evaluation of certified reference materials for Asian mineral dust. *Global Environ* Res **1**, 103–113.

Park, S., Park, M., and Chun, Y. (2010). Asian dust events observed by a 20-m monitoring tower in Mongolia during 2009. *Atmos Environ* **44**, 4964–4972.

Pelkmans, L. and Helenius, A. (2002). Endocytosis via caveolae. *Traffic* **3**, 311-320.

Ramachandran, G. (2011). Assessing nanoparticle risks to human health. Pp. 1–64. William Andrew publications, Elsevier's Science & Technology, Oxford, United Kingdom.

Rothberg, K. G., Heuser, J. E., Donzell, W. C., Ying, Y., Glenney, J. R. and Anderson, R. G. W. (1992). Caveolin, a protein component of caveolae membrane coats. *Cell* **68**, 673–682.

Sadauskas, E., Danscher, G., Stoltenberg, M., Vogel, U., Larsen, A., and Wallin, H. (2009a). Protracted elimination of gold nanoparticles from mouse liver. *Nanomedicine* **5**, 162–169.

Sadauskas, E., Jacobsen, N. R., Danscher, G., Stoltenberg, M., Vogel, U., Larsen, A., Kreyling, W., and Wallin, H. (2009b). Biodistribution of gold nanoparticles in mouse lung following intratracheal instillation. *Chem Cent J* **3**, 16.

Sadauskas, E., Wallin, H., Stoltenberg, M., Vogel, U., Doering, P., Larsen, A., and Danscher, G. (2007). Kupffer cells are central in the removal of nanoparticles from the organism. *Part Fibre Toxicol* **4**, 10.

Saunders, M. (2009). Transplacental transport of nanomaterials. *Wiley Interdiscip Rev Nanotech Nanobiotechnol* **1**, 671–684.

Semmler-Behnke, M., Kreyling, W. G., Lipka, J., Fertsch, S., Wenk, A., Takenaka, S., Schmid, G., and Brandau, W. (2008). Biodistribution of 1.4- and 18-nm gold particles in rats. *Small* **4**, 108–111.

Sonavane, G., Tomoda, K., and Makino, K. (2008). Biodistribution of colloidal gold nanoparticles after intravenous administration: effect of particle size. *Colloids and Surfaces B: Biointerfaces* **66**, 274–280.

Shimada, A., Kawamura, N., Okajima, M., Kaewamatawong, T., Inoue, H., and Morita, T. (2006). Translocation pathway of the intratracheally instilled ultrafine particles from the lung into blood circulation in the mouse. *Toxicol Pathol* **34**, 947–957.

Singh, S., Shi, T., Duffin, R., Albrecht, C., van Berlo, D., Höhr, D., Fubini, B., Martra, G., and Fenoglio, I. (2007). Endocytosis, oxidative stress and IL-8 expression in human lung epithelial cells upon treatment with fine and ultrafine TiO_2: role of the specific

surface area and of surface methylation of the particles. *Toxicol Appl Pharmacol* **222**, 141–151.

Shukla, R., Bansal, V., Chaudhary, M., Basu, A., Bhonde, R. R., and Sastry, M. (2005). Biocompatibility of gold nanoparticles and their endocytotic fate inside the cellular compartment: a microscopic overview. *Langmuir* **21**, 10644–10654.

Sung, J. K., Ji, J. H., Park, J. D., Song, M. Y., Song, K. S., Ryu, H. R., Yoon, J. U., Jeon, K. S., Jeong, J., Han, B. S., Chung, Y. H., Chang, H. K., Lee, J. H., Kim, D. W., Kelman, B. J. and Yu, I. J. (2001). Subchronic inhalation toxicity of gold nanoparticles. *Part Fibre Toxicol* **8**,16.

Takahashi, S., and Matsuoka, O. (1981). Cross placental transfer of ^{198}Au-colloid in near term rats. *J Radiat Res* **22**, 242–249.

Takata, K., Fujikura, K., Shin, B. (1997). Ultrastructure of the rodent placental labyrinth: a site of barrier and transport. *J Reprod Dev* **43**, 13–24.

Takenaka, S., Karg, E., Kreyling, W. G., Lentner, B., Möller, W., Behnke-Semmler, M., Jennen, L., Walch, A., Michalke, B., Schramel, P., Heyder, J., and Schulz, H. (2006). Distribution pattern of inhaled ultrafine gold particles in the rat lung. *Inhal Toxicol* **18**, 733–740.

Tratt, D., Frouin, R., and Westphal, D. (2001). April 1998 Asian dust event: a Southern California perspective. *J Geophys Res* **88**, 5343–5352.

Tsuchiya, T., Oguri, I., Yamakoshi, Y. N., and Miyata, N. (1996). Novel harmful effects of [60]fullerene on mouse embryos in vitro and in vivo. *FEBS Lett* **393**, 139–145.

Vega-Villa, K. R., Takemoto, J. K., Yáñez, J. A., Remsberg, C. M., Forrest, M. L., and Davies, N. M. (2008). Clinical toxicities of nanocarrier systems. *Adv Drug Deliver Rev* **60**, 929–938.

Warheit, D. B., Sayes, C. M., Reed, K. L., and Swain, K. A. (2008). Health effects related to nanoparticle exposures: Environmental, health and safety considerations for assessing hazards and risks. *Pharmacol Therapeut* **120**, 35–42.

Wick, P., Malek, A., Manser, P., Meili, D., Maeder-Althaus, X., Diener, L., Diener, P., Zisch, A., Krug, H. F., and von Mandach, U. (2010). Barrier capacity of human placenta for nanosized materials. *Environ Health Perspect* **118**, 432–436.

World Health Organization (WHO). (2003). Health aspects of air pollution with particulate matter, ozone and nitrogen dioxide. Report EUR/03/5042688 of working group, Bonn Germany, 13–15 January 2003. Copenhagan, Denmark: WHO Regional Office for Europe.

World Health Organziation (WHO). (2005). WHO Air quality guidelines for particulate matter, ozone, nitrogen dioxide and sulfer dioxide - Global update 2005 – Summary of risk assessment. Copenhagen, Denmark: WHO Regional Office for Europe.

Yamashita, K., Yoshioka, Y., Higashisaka, K., Mimura, K., Morishita, Y., Nozaki, M., Yoshida, T., Ogura, T., Nabeshi, H., Nagano, K., Abe, Y., Kamada, H., Monobe, Y., Imazawa, T., Aoshima, H., Shishido, K., Kawai, Y., Mayumi, T., Tsunoda, S., Itoh, N., Yoshikawa, T., Yanagihara, I., Saito, S., and Tsutsumi, Y. (2011). Silica and titanium dioxide nanoparticles cause pregnancy complications in mice. *Nature Nanotechnol* **6**, 321–328.

Yang, C., Tsai, S., Chang, C., and Ho, S. (2005). Effects of Asian dust storm events on daily admissions for asthma in Taipei, Taiwan. *Inhal Toxicol* **17**, 817–821.

Yang, W., Peter, J. I., and Williams III, R. O. (2008). Inhaled nanoparticles – a current review. *Int J Pharm* **356**, 239–247.

Yu, L. E., Yung, L. L., Ong, C., Tan, Y., Balasubramanium, K. S., Hartono, D., Shui, G., Wenk, M. R., and Ong, W. (2007). Translocation and effects of gold nanoparticless after inhalation exposure in rat. *Nanotoxicology* **1**, 235–242.

Zdanowicz, C., Hall, G., Vaive, J., Amelin, Y., Percival, J., Girard, I., Biscaye, P., and Bory, A. (2006). Asian dustfall in the St. Elias mountains, Yukon, Canada. *Geochim Cosmochim Ac* **70**, 3493–3507.